Monthly Weather Review

Large-eddy simulations of real world episodes in complex terrain based on ERA-Reanalysis and validated by ground-based remote sensing data
--Manuscript Draft--

Manuscript Number:	MWR-D-19-0016
Full Title:	Large-eddy simulations of real world episodes in complex terrain based on ERA-Reanalysis and validated by ground-based remote sensing data
Article Type:	Article
Abstract:	A computationally inexpensive approach for using the capabilities of large-eddy simulations to model small scale local weather phenomena is presented. The setup uses WRF-LES on a single domain that is directly driven by reanalysis data as boundary conditions. The simulated area is an example for complex terrain and the employed parameterizations are chosen in a way to represent realistic conditions during two 48 hour periods, while still keeping the required computing time on the order of 10^5 CPU hours. We show by evaluating turbulence characteristics that the model results conform to results from typical LES. A comparison with ground-based remote sensing data from a triple Doppler-Lidar setup, employed during the ScaleX campaigns, shows the grade of adherence of the results to the measured local weather conditions. The representation of mesoscale phenomena, including nocturnal low-level jets, strongly depends on the temporal and spatial resolution of the meteorological boundary conditions used to drive the model. Small scale meteorological features that are induced by the terrain, such as katabatic flows, are present in the simulated as well as in the measured data. This shows that the four dimensional output of WRF-LES simulations for a real area and real episode can be used for gaining a more comprehensive and detailed view of the conditions than with measurements alone.

Reviews to MWR-D-18-0243, Editor: Dr. Jidong Gao

Reviewer #1: Review on "LES simulations of real episodes in complex terrain and comparison with height-resolving ground-based remote sensing data" by Hald et al., 2018.

General comments:
This study conducted single-domain Large Eddy Simulations (LES) for 2 episodes over a 15km×15km area driven by ERA interim reanalysis boundary conditions with spectral nudging. The simulated wind speeds and wind directions are compared with Lidar measurements. The manuscript structure and English writing are good. While the Lidar data might be useful to evaluate LES outputs, the evaluation work reported in this manuscript has fatal issues.

1. The current evaluation of wind speeds and wind directions simulated by LES using Lidar data is actually meaningless because you are actually evaluating the ERA data at one grid point rather than actually evaluating LES' capability. The current domain (15 ×15 km) locates inside of one grid point of ERA interim data. Given the boundary condition forcing and spectral nudging forcing, the simulated wind speeds and directions in the domain is mostly inherited from the ERA data at this single grid. Thus, the model bias shown in this manuscript is actually dominated by the error in the ERA data at this single grid point.

- The purpose of the study is not the evaluation of LES capabilities but the application of the method to a known area with measurements present. For a meaningful comparison of the simulated data with measurements it is indispensable that the real boundary conditions are represented in the LES domain. ERA-Interim is considered to be a state-of-the-art data product to provide real boundary conditions to drive regional climate models. The alternative would be an idealized LES with constant boundary conditions. These LES are very suited for the evaluation of the LES capabilities, but not useful in representing real conditions.
- The boundary conditions do derive from a single grid point, yet there are distinct gradients in all input variables: The routines in WPS extrapolate the ERA data to the fine scale grid of the LES domain and the underlying elevation model change them further. This has now been explained better in the manuscript (Lines 155-158).

2. Application of spectral nudging is problematic:
The idea of spectral nudging is that we trust the driving forcing (ERA data in this case) in reproducing the large-scale meteorological fields and thus we nudge mesoscale/small-scale simulations to the driving forcing in those large scales.
We don't know at what scale the spectral nudging is applied to in this study since it is not mentioned in the manuscript, but it has to be less than 15 km (domain size). However, given the grid spacing of ERA data, 0.7o, there is no way the ERA data could faithfully reproduce the meteorological fields at wavelength of 15 km or smaller. Thus application of spectral nudging in this case is invalid. Actually spectral nudging in this study will seriously suppress small-scale features generated by model dynamics and bring in model errors inherited from the driving fields at this grid point.

- We have repeated all simulations without the application of nudging. All numbers and figures that are now presented in the draft refer to the data simulated without nudging.
- We have checked the differences in the two datasets, yet did not find substantial changes. For example, the magnitudes in the wind component time series in model resolution show very similar means and variances. Differences can be observed only due to the intrinsic variability of turbulence (i.e. an eddy is passing by at a different time). Accordingly, these differences are higher during day when turbulence is pronounced.
- When averaging over several minutes, the solutions of our runs with and without nudging converge even more.
- We also could only observe such differences in the spatial distribution of variables that are

also attributable to natural variability of turbulence. There were no systematic changes in wind fields etc. between simulations without and with nudging.

- Yet, we are thankful for the hint that nudging might interfere with the solutions. Our new simulations have removed this factor of uncertainty.

Other minor comments
1. Introduction is a little bit weak to present the current research status of WRF-LES and the motivation is not strong:
A few studies have used WRF-LES (e.g., Chu et al., 2014; Mirocha et al., 2013; Mirocha et al., 2014; Rai et al., 2017). Why do we need this one?

- The list of studies on LES has been supplemented with more references. As for the necessity of this study, we now put more focus on the fact that we present a comparatively lower cost LES application that does have additional benefit to mesoscale models due to being able to compare the model results with measurements of boundary layer dynamics (Lines 101-116).

The 3rd objective (i.e., LES is valuable addition to measurements) is not unique to LES, all the mesoscale/small-scale simulations do. The reviewer does not think this is the contribution from this study.

- We are convinced that LES brings more benefit than mesoscale models due to the high spatio-temporal resolution, especially when comparing to measurements from different heights. High vertical resolution, as e.g. provided by virtual towers, cannot be sufficiently resolved by mesoscale models. Only vertically integrated (i.e. averaged) values could be compared. With LES, the entire column can be compared. We have substantiated this in the manuscript.

The title of this paper mentions the complex terrain, however, in the introduction, the authors are failed to provide related background information about it and motivation about why study in complex terrain rather than other regions.

- We have better explained now why we think it is current forefront of research to setup, apply and evaluate Large Eddy Simulations for real episodes in complex terrain. The main reason is that very flat and homogeneous surfaces are adequate for some process studies, but not representative for most of the earth's surface. We also focus on what needs to be considered when setting up WRF-LES with a DEM. These steps in the model setup are rarely, if ever described, as they are part of the preliminary work. We think it is the forefront of research to address realistic complex terrain areas in LES. We have changed the description in the introduction (lines 93-98)

Specific comments
1. line 1. "LES simulation", since LES has included simulation, therefore simulation is extraneous. Many other places have this issue.

- The redundant „simulation" has been removed from all instances where this mistake happened, including the title.

2. Line 32, eddys should be eddies

- This has been changed in the new manuscript (line 34).

3. line 38, 1970ies?

- The relevant part has been re-phrased (line 38).

4. lines 49-52, which point are you want to address in this paragraph?

- With this, we meant to distinguish between LES with constant, idealized conditions and such with variable conditions (wind fields, temperature profiles). The paragraph has been supplemented with a sentence to clarify (lines 50-52).

5. line 80, LES simulation issue
- see point 1.

6. line 92, You have defined WRF too many times
- The surplus definition of WRF has been removed.

7. line 100, full name of a.s.l.?
- A definition of „a.s.l." (above sea level) has been added (line 131).

8. line 144-145, incomplete sentence, to what?
- The virtual tower data is compared to the simulated data. The sentence has been re-phrased to make it more precise (lines 171-172).

9. lines 168-184. You need explain the height limit of the observation for Lidar and why (since you mention it in the result part). Also the detailed information about the Doppler-Lidar (e.g., which type? Which company?) should be given.
- We have now added the model and manufacturer information "...(model StreamLine XP, Halo Photonics Ltd, Worcester, England).' (line 205)
- The maximum profile height retrieved from the lidar measurements was in first place determined by instrument specifications (up to 3 km). But in practice there were other obstacles, including the quality of the backscattered signal (deteriorating with distance from the instrument and in layers with fewer particles), the configuration of the scan routine (a linear angular scan velocity) in combination with the vertical resolution chosen for computation of profiles, as well as the elevation angle of the beams combined at the profile intercept. Based on the reviewers comment, we have changed the sentence: l169: "The vertical resolution is 3 m up to a height of about 20 m above ground and 18 m up to a 1000m above ground, depending on atmospheric conditions." to "The vertical resolution is 3 m up to a height of about 20 m above ground and 18 m up to a 1000 m above ground. The range above 1000 m was excluded because of detection limitations, thought to be related to a decrease in particle density away from the surface that leads to decrease in backscattered laser light signal." (lines 212-215)

10. line 191, by turbulence by buoyancy?
- „by turbulence" has been discarded, leaving „[...] a boundary layer that is driven by buoyancy".

11. line 406, what is cfl-criterion?
- This describes the Courant-Friedrichs-Lewy condition. The relevant part has been changed and the source for the condition has been added (line 539-540).

12. LN100-102, "unevenly" contradict "11m", Explicitly showing vertical resolution would be helpful.
- The layering of the vertical levels has been explained in more detail (lines 131-133). We hope this is sufficient, without the addition of an additional figure.

13. LN202-203, how does the PBL height derived?
- The PBL height by day was derived by using the gradient method described by Sullivan et al. (1998, JAS). The sentence this part was in has been removed, and information about PBL heights and their derivation can be found in the paragraph above (lines 233-234 and 255-256). Our derivation of the nocturnal BL height can be found in lines 324-330.

References:
Chu, X., Xue, L. L., Geerts, B., Rasmussen, R., & Breed, D. (2014). A Case Study of Radar Observations and WRF LES Simulations of the Impact of Ground-Based Glaciogenic Seeding on Orographic Clouds and Precipitation. Part I: Observations and Model

Validations. Journal of Applied Meteorology and Climatology, 53(10), 2264-2286. 10.1175/Jamc-D-14-0017.1
- A citation for this study has been added at the appropriate location, along with its subsequent study by Xue et al. 2016 (line 69).

Mirocha, J., Kirkil, G., Bou-Zeid, E., Chow, F. K., & Kosovic, B. (2013). Transition and Equilibration of Neutral Atmospheric Boundary Layer Flow in One-Way Nested Large-Eddy Simulations Using the Weather Research and Forecasting Model. Monthly Weather Review, 141(3), 918-940. 10.1175/Mwr-D-11-00263.1
- This study had already been cited in the original manuscript as an example for nesting a LES domain in another LES domain (line 65). It now occurs again at line 266 as a reference for streaks of under-developed turbulence at domain edges.

Mirocha, J., Kosovic, B., & Kirkil, G. (2014). Resolved Turbulence Characteristics in Large-Eddy Simulations Nested within Mesoscale Simulations Using the Weather Research and Forecasting Model. Monthly Weather Review, 142(2), 806-831. 10.1175/Mwr-D-13-00064.1
- A citation is added where we write about other studies using WRF-LES (line 67) and as a source for the fact that turbulence within a single domain can develop through slopes and heat fluxes (line 282).

Rai, R. K., Berg, L. K., Kosovic, B., Mirocha, J. D., Pekour, M. S., & Shaw, W. J. (2017). Comparison of Measured and Numerically Simulated Turbulence Statistics in a Convective Boundary Layer Over Complex Terrain. Boundary-Layer Meteorology, 163(1), 69-89. 10.1007/s10546-016-0217-y
- This study had already been cited in the original manuscript as a good example for the application of WRF-LES on realistic conditions (line 89/90).

Reviewer #2: Review of the manuscript "LES simulations of real episodes in complex terrain and comparison with height-resolving ground-based remote sensing data" by Cornelius Hald, Matthias Zeeman, Patrick Laux, Matthias Mauder and Harald Kunstmann submitted for publication in the Monthly Weather Review.

In the manuscript "LES simulations of real episodes in complex terrain and comparison with height-resolving ground-based remote sensing data" the authors present an evaluation of large-eddy simulations of a diurnal cycle of an atmospheric boundary layer based on a field study using three doppler lidars. The LES are forced directly by initial and boundary conditions derived from ERA Interim reanalysis. Spectral nudging is applied before boundary condition update to provide more smooth transition. LES results are in general in a good agreement with observations demonstrating the ability of LES to capture processes in a boundary layer over a complex terrain.

General Remarks

In general, the manuscript is written well and the numerical study is well designed. The approach to force LES directly with initial and boundary conditions derived from a reanalysis is not common, however, the results presented in the study support the authors choice. This choice is justified by the fact that the terrain outside LES domain is very complex and nesting LES within mesoscale simulation is not a good option. Demonstration that forcing LES with initial and boundary conditions derived directly from reanalysis (or a global model) is viable can be useful for future studies. Furthermore, the results demonstrate that high-resolution simulations (i.e. LES) provide additional information about local flows affected by terrain features that could be of importance for various applications.

The diurnal cycle is simulated using one LES domain with 30 m horizontal resolution and high vertical resolution. This is a limitation of the study, because at 30 m stably stratified ABL is not well resolved. More detailed analysis (e.g., spectral analysis) would show that most of the turbulence during nighttime stable conditions is not resolved. Either evidence to the contrary should be presented or this should be stated in the manuscript.
- We agree that a horizontal resolution of 30 m might not be sufficient to fully resolve the turbulence within a stable NBL. We have added a figure showing spectra of two phases during day (strongly and weakly convective) and one during night (figure 5). We conclude in an added paragraph that some but not all possible scales of turbulence are resolved and that a higher resolution is needed if turbulence characteristics of the stable boundary layer are the main focus of the simulation (lines 347-349).

Better approach would have been to use LES nested within LES during nighttime. Furthermore, considering that lidar measurements can provide estimates of TKE and velocity spectra (see Bodini et al. 2018, AMT), it would be appropriate to present at least a limited comparison of simulated turbulence quantities to observations.
- We have tried adding a nest at the location of the virtual tower, yet could not find a working configuration. The simulation crashed within the first few time steps at the nests' edges. As our focus was also the description of a computationally low-cost LES we did not pursue this approach further.
- We thank the reviewer for the suggestion. In common single lidar instrument operation these turbulence properties can indeed be computed as described in literature and a comparison with model results would be informative here. During the observational days in this study, a multiple unit scan routine was used for which turbulence statistics cannot be computed, or would require methods that have not been validated yet. We therefore cannot add a comparison. However, our Lidar virtual tower measurements offer the advantage of providing 3D wind across the boundary layer without the assumption of horizontal homogeneity of the wind field at a given height.

In addition there are a few omissions and a few statements, listed under specific remarks, that need to be modified or corrected.

Taking all the above into account I recommend the paper for publication in the Monthly Weather Review after my comments and suggestions for major revision are addressed.

Specific Remarks

Line 37 - This is not accurate. Turbulence parameterizations in mesoscale models represent Reynolds stress, in LES what is represented is subgrid stress includes a Reynolds stress like component.
- The specified sentence has been removed and a different explanation for the SGS model has been added in the sentence before (line 37-38).

Line 39-40 - Instead of Moen 1986, better (earlier) reference for an LES of a convective boundary layer would be Moeng 1984 (JAS).
- The proper reference has been inserted (line 41).

Lien 59 - Preceding Lang et al. (2015) was Nunalee et al. (2014, Atmos. Environ.).
- The citation for Nunalee et al. has been added at the appropriate location (line 63).

Line 62 - Instead of "about" it should be "of."
- „about" has been substituted with „of" (line 71).

Line 67 - The statement: "… at confined location or at different places at different times…" should be restated in a more concise and clear way.
- This has been done as requested (line 76-79).

Line 68 - The statement "Until now, only few studies on realistic conditions with WRF-LES exist; two examples are Talbot et al. (2012), who evaluate the influence of different resolutions on the results for a LES of an urban area and Rai et al. (2017)." Is not quite accurate. There are more than just a few studies, the list is could include: Munoz-Esparaza et al. 2014 (BLM), 2017 (JAMES), 2018 (JAMES and MWR), as well as Aitken et al. 2015 (JRSE) motivated by observations.
- We highly appreciate the hint to Muñoz-Esparza et al. 2017 (JAMES). It has been added to the appropriate paragraph (line 91). We argue that the studies presented in Muñoz-Esparza et al. 2014 in BLM and 2018 in JAMES, as well as Aitken et al. 2015 do not represent the application of WRF-LES on realistic but on idealized conditions. They have therefore been added as additional references where we write about the application of WRF-LES in general (lines 66,68). Muñoz-Esparza et al. 2018 in MWR evaluate the turbulence dissipation in PBL schemes, using resolutions above LES scales.

Line 103 - This is not "inaccuracy" since this is a feature of WRF - better term would be "variability."
- The word has been changed. Additionally, the sentence before that has been re-phrased in order to better explain the layering of the vertical levels (lines 131-135).

Line 127-128. Turbulence development should be confirmed in some way, e. g. looking at spectra at different locations and potentially comparing simulated spectra to observed.
- This sentence has been removed from this chapter. We have added a paragraph in the results chapter (lines 291-305) where we show that turbulence does develop in the domain, mostly due to the variance in terrain and varying surface heat fluxes.

Line 177 - LES is supposed to resolve turbulent eddies with characteristic time scale less then 1 minute, including inertial scale eddies, why would then highest resolution for reliable values be only 1 minute?
- This sentence is in the section that treats the measurements taken by the virtual tower. It

does not describe a property of the simulation data. The scanning mode used in the device averages measurements over at least a minute.

Line 191 - Instead of "by turbulence by buoyancy" this should probably be just "by buoyancy."
- This has been changed.

Line 193 - Cell like structures depend on the stability parameter z_i/L. When z_i/L > -20 then the dominant boundary layer structures are convective rolls (see for example LeMone et al. (JAS 1976).
- The calculated values of z_i/L are now presented in the according paragraphs. In the case of low wind speeds the values hint at cells. During high wind speed we found that the bulk of the grid points have z_i/L values between 0 and -10, meaning the possibility of roll-like structures. We also hint at the fact that in such an inhomogeneous domain and during a convective phase, strongly unstable conditions can be found next to moderately stable or even neutral grid points. The stability cannot be defined for the whole domain.

Line 199 - If 2000 m is the ABL height then this can be expected.
- The area of shear is not the height of the boundary layer. The PBL height derived by using the gradient method shows that it is between 500 and 700 m above ground. We have added this to the manuscript (lines 253-256).

Line 215 - "Exponentially" has a very precise mathematical meaning that would have to be shown in this case. Since this was not done, better would be to say "significantly."
- The word „exponentially" has been replaced with „significantly" (line 289).

Line 226-227 - More details should be given about specific windowing function. Also, why not Hann or Hamming window?
- A cosine bell taper is described as one of the more common methods for a smoothing function in Stull (1988). Details for the function have been added to the according paragraph (line 299-300). See the figure below on how the data is influenced by the two different functions. We argue that the Hamming window changes almost all values in the time series, while the cosine bell taper is only applied to the first and last 10% of the data. This leaves more of the dynamics intact. This is important since our time series are only 2 hours long in order to have constant meteorological conditions.
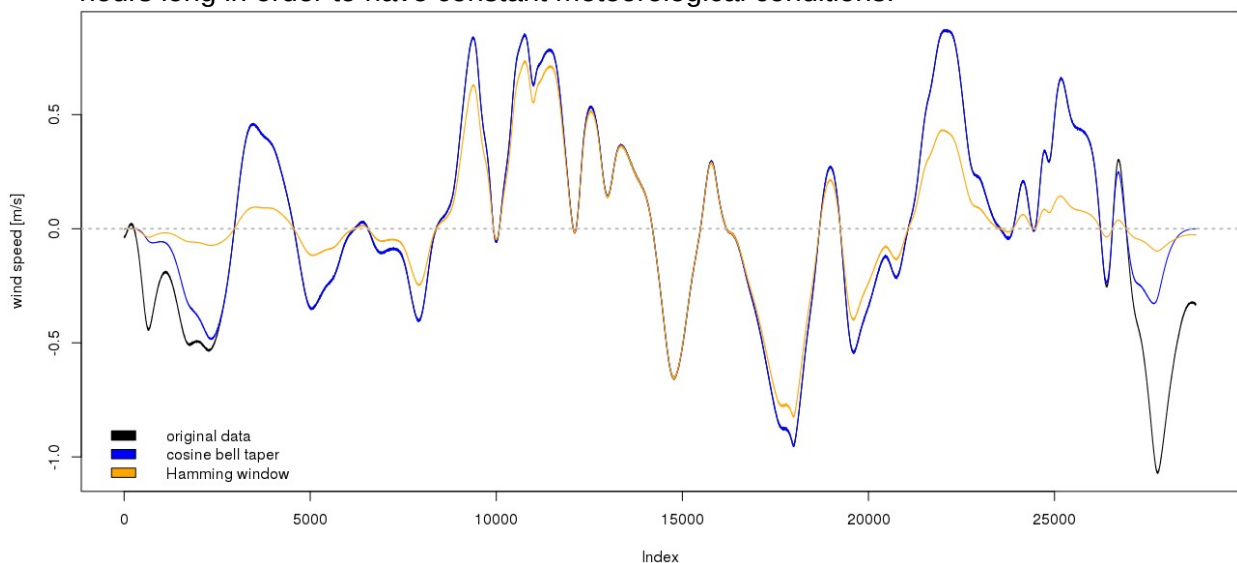
Line 231 - Instead of "on" it should be "at."
- The whole paragraph has been changed.

Line 232 - Instead of "inertial subrange is small..." more precisely would be "resolved inertial range is short..."
- The whole paragraph has been changed.

Line 254 - Here, "disappear" is not an appropriate term. The ABL transitions to a daytime, convective boundary layer.
- The sentence has been re-phrased (line 369-370).

Line 265-266 - Actually, the nose of the LLJ usually coincides with the ABL top.
- We changed the sentence. Yet, from our understanding, the LLJ is more like a sheet of fast moving air above the NBL and therefore has no nose.

Line 302 - It would be important to be consistent and use only single letters to denote wind directions or spell out the words, but not mix the two (c.f. lines 70, 199, 386 vs. 204, 244, 246, 249, 250)
- Directions have been standardized. They all are „northwest", „southeast" etc. now.

Line 330 - I do not think that it is appropriate to say that nocturnal boundary layer is "lifted." Another term, like "erosion of the nocturnal..."
- This has been changed as recommended (line 449).

Line 400 - The acronym LES should be used here.
- This has been changed as recommended (line 532).

Line 413-415 - This sentence is not clear, there seem to be two distinct statements and perhaps these should be separated. The first statement is essentially repeated in the next sentence and therefore could be omitted.
- The whole paragraph has been clarified (lines 545-557).

Line 416 - Instead of "time steps" it should be "time periods."
- The whole paragraph has been changed.

Reviewer #3: Reviewer's comments on "LES simulations of real episodes in complex terrain and comparison with height-resolving ground-based remote sensing data"

It has been well recognized that the nesting from mesoscale to LES models helps to improve local weather prediction at very high resolution. The validation using advanced observed data is necessary for improving the modelling systems and for understanding the fine-scale features of weather phenomena and associated physical processes. This study uses WRF-LES to simulate several different features (turbulence, diurnal cycle of the boundary layer, and katabatic flow) in the realistic atmospheric and surface conditions. Part of the model results especially on diurnal cycle of the boundary layer is compared with the data retrieved by Doppler windlidar systems. However, there are several major concerns that need to be addressed. In particular, the multiscale phenomena of turbulence and weather conditions should be connected with more in-depth analyses.

1. This study examines several different features in a manner that they appear to be not closely related with each other and the address on each topic is lack of in-depth analyses. For instance, Figures 2-4 show the different turbulent activities occur in the simulation with different dynamic conditions. It should be quantitatively validated using the observation data at hand. The causes of the differences in two episodes and those between simulation and observation should be discussed in detail with more evidence. It is recommended to focus on a few phenomena so that the quantitative estimation of model bias is possible, particularly regarding the fine-scale structures that are well resolved at LES resolution.
- We clarified the manuscript in order to better link the different parts: We describe a computationally low cost LES setup for a real area, then evaluate the model output separately to show that LES conditions (developed turbulence) is reached. In the next step we show that it is, under these circumstances possible to reproduce the measured quantities in wind. A detailed phenomenon is discussed in the part about the katabatic flow, which has been complemented by a figure showing the temperature deviations, as you requested in your point 4.
- An in-detail comparison of turbulence metrics was not possible due to the scan mode the Lidar system was used in. This does not allow for computing turbulence measures.

2. There are several issues that may responsible for the forecast bias of the nested mesoscale-LES models: the background of atmospheric conditions, the influence of underlying surfaces conditions (inhomogeneous land-use and topography), and the transition from smooth mesoscale inflow to turbulence resolved in inner domain. When all these conditions are well treated in the models, they may improve the prediction of local weather. For a reasonable growth of turbulence in inner model, some treatments like artificial perturbations is needed to ensure the realistic reproduction of turbulence (e.g., Muñoz-Esparza and Kosović 2018, https://doi.org/10.1175/MWR-D-18-0077.1). A reliable weather condition may be achieved using data assimilation in mesoscale model and help to reproduce the general features of turbulence in the LES domain (e.g., Chen et al. 2015, https://doi.org/10.1175/MWR-D-14-00212.1). A careful design of the simulations may inhibit the presence of under-resolved convection at convection-resolving mesoscale resolution and to ensure proper turbulence representation in stably-stratified conditions (e.g., Muñoz-Esparza et al. 2017, https://doi.org/10.1002/2017MS000960). As this study emphasizes the LES modeling of realistic weather conditions, a discussion on these related factors will help to improve the quality. For instance, in Figures 2-3, the regional differences of turbulence are shown to relate to the terrains, so the detailed examination on the possible topography influence is expected to clarify this interesting phenomenon. In Figures 3a,d, from north to south, there is a transition of smooth inflow to roll convection and cell convection.
- The authors thank you for pointing them into the direction of making sure that proper turbulence is developed within the domain. We understand that the method of perturbing temperature fields at the domain edges, as proposed by Muñoz-Esparza et al. (2014) and Muñoz-Esparza and Kosović (2018) does improve the development of turbulence, yet this

approach is not implemented in WRF and the development of an implementation would have been beyond the scope of this study.
- The approach by Chen et al. 2015 is assumed to require enormous amounts of computing power, while we tried to focus on using a low amount. We have clarified this in the document.
- Having a nest with a higher resolution at the location of the virtual tower in order to resolve SBL turbulence, as described by Muñoz-Esparza et al. 2017, showed to lead to even more instabilities in our model. It would also have increased the computing time considerably, foiling our attempt to keep the computing costs low.
- In order to show that turbulence does develop within the domain during day we have added spectra of five locations within the domain (figure 4), one within the area of visibly under-developed turbulence, the others on the same longitude. It shows that only the one location shows a spectrum different from the others. A comparison of day and night spectra is also added (figure 5). This shows that turbulence is developed during day, but in different shapes depending on the stability, while nighttime turbulence is under-developed.

3. The interaction between weather condition and turbulence is another important issue. In this study, how are the modeling on the diurnal cycle of boundary-layer wind related to the simulation of turbulence using LES. As for the katabatic flows, they are formed at local orography but may be insensitive to the ambient winds at least for the effect on downstream area. Using WRF-LES, it is possible to clarify the turbulent flows and their interaction with environment in the realistic weather conditions.
- The main focus of the study is the representation of local weather on a high resolution scale. We think this resolution adds benefit over mesoscale models because it resolves boundary layer dynamics that would otherwise be parameterized. It is on a scale that allows for in-depth comparison with height resolving measurements. The focus was not on the evaluation of turbulence dynamics. Yet, we did add a detailed evaluation of the turbulence characteristics in oder to prove that the model exhibits LES properties to make sure that the subsequent evaluations are based on correct data.
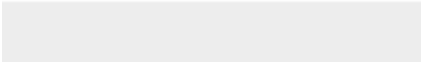
4. Regarding the katabatic flows, some plots on the temperature disturbance may help to illustrate the structures and temporal evolution of cold pool.
- Thank you for this suggestion. Such a figure has been added (figure 13) and it indeed shows the development of a cold-pool as well as its depletion during later hours.

Track-Changes Version of the manuscript

Click here to access/download
Additional Material for Reviewer Reference
track_changes.pdf

Large-eddy simulations of real world episodes in complex terrain based on

ERA-Reanalysis and validated by ground-based remote sensing data

Cornelius Hald*, Matthias Zeeman, Patrick Laux, Matthias Mauder and Harald Kunstmann[†]

Institute of Meteorology and Climate Research (IMK-IFU), Karlsruhe Institute of Technology (KIT), Kreuzeckbahnstr. 19, 82467 Garmisch-Partenkirchen, Germany.

Corresponding author address: Institute of Meteorology and Climate Research (IMK-IFU), Karlsruhe Institute of Technology (KIT), Kreuzeckbahnstr. 19, 82467 Garmisch-Partenkirchen, Germany.

E-mail: cornelius.hald@kit.edu

[†]Institute of Geography (IGUA), University of Augsburg, Germany.

ABSTRACT

A computationally inexpensive approach for using the capabilities of large-eddy simulations to model small scale local weather phenomena is presented. The setup uses WRF-LES on a single domain that is directly driven by re-analysis data as boundary conditions. The simulated area is an example for complex terrain and the employed parameterizations are chosen in a way to represent realistic conditions during two 48 hour periods, while still keeping the required computing time on the order of 10^5 CPU hours. We show by evaluating turbulence characteristics that the model results conform to results from typical LES. A comparison with ground-based remote sensing data from a triple Doppler-Lidar setup, employed during the ScaleX campaigns, shows the grade of adherence of the results to the measured local weather conditions. The representation of mesoscale phenomena, including nocturnal low-level jets, strongly depends on the temporal and spatial resolution of the meteorological boundary conditions used to drive the model. Small scale meteorological features that are induced by the terrain, such as katabatic flows, are present in the simulated as well as in the measured data. This shows that the four dimensional output of WRF-LES simulations for a real area and real episode can be used for gaining a more comprehensive and detailed view of the conditions than with measurements alone.

2

1. Introduction

Large-eddy simulations (LES) are a tool for studying turbulent motions in the atmosphere. By using a model resolution of 100 m or smaller, the large turbulent motions can be explicitly resolved. This part of the turbulence represents the inertial subrange (e.g. Stull 1988), a range in which the turbulent energy is passed on from larger to smaller eddies. All structures smaller than a certain filter width, usually dependent on the model resolution, are parameterized in a LES, assuming that turbulence on very small scales is close to being isotropic, a prerequisite for the application of a parameterization. A subgrid-scale (SGS) model is responsible for the representation of all turbulent motions smaller than the filter and the dissipation of kinetic energy into heat.

LES have been used since around 1970 (Deardorff 1970), starting with the application of such models to neutral (Deardorff 1972; Andren et al. 1994; Beare et al. 2006) or convective (Moeng 1984, 1986; Nieuwstadt et al. 1993; Siebesma et al. 2003) boundary layers due to the relatively large size of the turbulent motions under those conditions. With growing access to extensive computing resources and the ability to improve the resolutions in LES to resolve turbulence on the smallest scale, studies for stable boundary layers were conducted (Kosović and Curry 2000; Saiki et al. 2000; Basu and Porté-Agel 2006; Huang and Bou-Zeid 2013). Most of these applications of LES used idealized initial and boundary conditions, representing flat and homogeneous or regularly patched surfaces (Bou-Zeid et al. 2004) or ideal valleys (Wagner et al. 2015). Moreover, the meteorological drivers were mostly idealized and periodic, with constant winds or prescribed temperature profiles.

In recent years, LES studies with real-world conditions have emerged. In contrast to the studies of flat and homogeneous terrain listed above, these try to approach non-idealized conditions: they use non-flat surfaces, changing heat fluxes, wind speeds or temperature profiles. Some examples

are the examination of a flow over a realistic hill (Chow and Street 2009), the transition from a stable to a convective boundary layer in the morning hours (Beare 2008) or the flow over urban structures (Bou-Zeid et al. 2009). The studies listed up to this point use model systems specifically designed as large-eddy simulation frameworks. They often lack the capabilities of weather models, especially in the area of nesting and specifying boundary and initial conditions to represent real weather conditions at certain locations.

The study presented here uses the LES capabilities of the Weather Research and Forecasting Model (WRF, Skamarock et al. 2008). Some applications of WRF-LES are, for example, the simulation of a daytime boundary layer in an idealized valley (Catalano and Moeng 2010) or a neutral boundary layer (Hattori et al. 2010), the simulation of the sea breeze (Crosman and Horel 2012) or the evaluation of the transport of passive tracer gases around a solitary hill (Nunalee et al. 2014) and of pollutants over a mountain range (Lang et al. 2015). The effects of nesting a LES domain in another was described by Moeng et al. (2007) and Mirocha et al. (2013). Muñoz-Esparza et al. (2014a) nest a LES representing a convective maritime boundary layer in an ideal LES. Nesting of LES in a mesoscale simulation is described in Mirocha et al. (2014). Aitken et al. (2014) present a module for the representation of wind turbines that can be used in WRF-LES, Chu et al. (2014) and Xue et al. (2016) evaluate how silver iodide is spread when released in the atmosphere.

While the idealized LES were mostly performed for investigations of the structure of turbulence in the atmosphere and for improving the boundary layer parameterizations in mesoscale models, LES for realistic conditions serve a different purpose: if the LES results are proven to sufficiently represent the real conditions at the simulated location, they provide a realistic four dimensional picture of the flow structures. Therefore, LES can be a helpful addition to the interpretation of spatially sparse observational data. Observational stations are often confined to few stationary lo-

4

cations, hence do not collect dense information in space, whereas moving measurement platforms (e.g. planes and drones) can gain spatial information, on the expense of the temporal information. Model data has information in all dimensions.

Due to its origin as a mesoscale weather and climate model, WRF already has many parameterizations and sub models implemented. WRF additionally comes with a pre-processing system (WPS) for providing boundary conditions.

Realistic conditions in a weather model are approximated when the model simulates the diurnal changes to radiation, when it uses information on land use, land cover and elevation, when moisture in the air is considered and when the boundary conditions represent real weather. This is costly in WRF-LES: every module that is switched on in addition to the fluid dynamics computations increases the required computing time significantly. Until now, only few studies on such realistic conditions with WRF-LES have been performed; examples include Talbot et al. (2012), who evaluate the influence of different resolutions on the results for a LES of an urban area and Rai et al. (2017), who simulated a rural area in the northwestern US and compared model outcomes to measurements. Muñoz-Esparza et al. (2017) nested realistic LES domains in three mesoscale domains and compared model outcomes to measurements.

In this study, we use WRF-LES to simulate two real-world episodes over complex terrain, characterized by height differences of 440 m, slopes of up to 20 $^\circ$ and varying soil properties that influence friction and the heat and moisture fluxes. The area is an example for a place dominated by agriculture in the temperate regions of central Europe. Studying complex terrain is necessary to allow a wider range of opportunities for LES in real world micrometeorological investigations. The simulated periods contain the transitions from nocturnal to daytime boundary layers and vice versa. The model results are evaluated against measurements of wind profiles using a triple Doppler-Lidar setup.

The first objective of this study is to analyze and evaluate model setups to achieve a stable model run in WRF-LES when using realistic boundary conditions and parameterizations over complex terrain. The second objective is, in its first part, to evaluate if WRF-LES with the computationally inexpensive configuration presented here (driving the LES domain directly with reanalysis data as boundary conditions) is able to produce results that are representative for a LES. In the second part we show by comparing to virtual tower measurements that WRF-LES is able to reproduce the mean quantities of the wind fields measured. Only typical LES data resolution is high enough that it can resolve the strong variability of wind properties with height and allows for a detailed comparison with measurements that exceeds the simple inspection of averages. As a third objective, we demonstrate how a LES for a known area is a valuable addition to measurements, by analyzing a katabatic flow event. The four dimensional model output shows the origin and development of the flow due to the influence of the terrain and therefore allows a much deeper insight in the local meteorological conditions compared to the measurements alone. This is not possible with weather models in mesoscale resolution, yet this configuration of WRF-LES is able to produce the detail necessary while using about one order of magnitude less in processing power than nested simulations.

Chapter 2 contains the setup of the WRF-LES model and information about the measurement principles of the Doppler-Lidar. Chapter 3 describes and discusses the results of the simulations and the grade of agreement between model and measurements and shows how realistic LES can complement measurements. The article ends with concluding remarks in chapter 4.

2. Methods

a. Model setup

The Weather Research and forecasting Model (Skamarock et al. 2008) has its origin in simulating the weather and climate for the macro- and mesoscale for operational and research purposes. It contains a refined pre-processing system (WPS) with the ability to create input and boundary files representing realistic conditions. It offers parameterizations for microphysics, radiation and land-surface processes and also the possibility of nesting. Many of these can also be applied when running WRF in LES mode. Version 3.7.1 of the model code was used. It was run in a single domain configuration. The domain covers 15 by 15 km with 500 grid points in x and y direction, meaning $\Delta x = \Delta y = 30$ m. In z direction the model reaches up to 500 hPa at around 5500 m a.s.l. (above sea level) and is split into 150 vertical levels. The height intervals are unevenly distributed: the first 105 levels have a resolution of ≈ 11 m. Above this, the vertical resolution becomes coarser with height, reaching ≈ 100 m in level 130 and ≈ 150 m in the topmost level. The variability in the heights of the vertical levels results from WRF's pressure based vertical levels and the terrain following coordinates. Due to the complexity of the terrain surrounding the area of interest it was not possible to find model configurations that nest the LES domain into other LES domains (e.g. following Talbot et al. 2012) or in mesoscale domains with parameterized boundary layers (e.g. following Rai et al. 2017). The vertical resolution of 11 m would have led to high aspect ratios between Δx and Δz, which through high slope angles could lead to model instabilities (Lundquist et al. 2010). The vertical nesting in WRF (Daniels et al. 2016), officially implemented in version 3.8 of the model code, could already be used in 3.7.1, but due to limitations concerning the available parameterizations when nesting vertically, this approach was not pursued further here.

₁₄₃ Within the top 500 m of the model domain, there is a Rayleigh damping layer to cope with the

₁₄₄ sound waves originating from the fact that WRF solves the fully compressible equations of motion

₁₄₅ (Moeng et al. 2007) and therefore explicitly resolves motions due to pressure changes. Many other

₁₄₆ LES codes apply the Boussinesq-Approximation in order to simplify the equations.

₁₄₇ The simulation included the periods 15-17 July 2015 and 6-8 July 2016. Both 48 hour peri-

₁₄₈ ods were selected because they both were times of high incoming solar radiation with moderate

₁₄₉ geostrophic winds, meaning that the turbulent structures during the day are large and the exchange

₁₅₀ processes are mostly driven by buoyancy. No precipitation was observed during the dates and in

₁₅₁ the selected study area.

₁₅₂ The model domain was initialized with atmospheric boundary conditions taken directly from

₁₅₃ the ERA interim reanalysis (ECMWF 2009, updated monthly). This dataset is in T255 horizontal

₁₅₄ resolution, spanning about 0.7 °. That means that the input data created by WPS for a 15×15 km

₁₅₅ domain is practically taken from a single grid point in the reanalysis. Due to the interpolation

₁₅₆ routines used by WPS for the meteorological input there are gradients present in the initial and

₁₅₇ boundary conditions. Both are additionally modified by the high resolution terrain in the domain,

₁₅₈ introducing further variability. Meteorological boundary conditions were updated every 6 hours.

₁₅₉ Land use classification data is taken from the 28-category Corine land use dataset in 3 arc second

₁₆₀ resolution (CLC 2000); the digital elevation model (DEM) is taken from the 1 arc second ASTER

₁₆₁ dataset (NASA/METI/AIST/Japan Spacesystems and U.S./Japan ASTER Science Team 2009).

₁₆₂ The domain is centered around 47.823 °N and 11.079 °E and is located in southern Germany

₁₆₃ (Figure 1a). Within the domain the elevation ranges from 520 m to 960 m a.s.l. (Figure 1b). The

₁₆₄ eastern part is characterized by relatively flat terrain. To the west, a plateau rising the terrain to

₁₆₅ above 700 m can be found. On the southern part of the plateau lies a mountain with a maximum

₁₆₆ height of 962 m, followed by a narrow valley in the southwestern part of the domain. Further

information on the area can be found in Wolf et al. (2017). The eastern flank of the mountain, which is coinciding with the ridge, leads to a steep slope in the terrain. Angles of about $30°$ in connection with WRF's terrain following coordinates result in numerical instabilities (Lundquist et al. 2010). The DEM therefore was smoothed until the maximum slope angles were at $20°$. The black circle in Figure 1b shows the location of the virtual tower device. The measurements of this device are used for the evaluation of the simulated data (see section b for details). It was not possible to center the domain around this location due to a gorge to the immediate west of the domain and mountains to the southwest. These features would have required a very extensive usage of smoothing of the input data that would have meant a great loss of information.

The WSM 5-class microphysics scheme (Hong et al. 2004) was used in combination with the RRTMG scheme for long- and shortwave radiation (Iacono et al. 2008), updated every four model time steps. Noah LSM was used as the land-surface model and Monin-Obukhov (MO) similarity governed the exchange between surface and atmosphere. It was described by Basu and Lacser (2017) that MO should not be used if the lowest vertical level is below a multiple of the roughness elements. The lack of other options in WRF made its use necessary. To reduce its influence, the lowest model level was not included in the evaluation. The diffusion coefficients were calculated by the 1.5 order TKE-closure in three dimensions and the subgrid processes were parameterized by the NBA-model with the TKE based stress terms (Kosović 1997; Mirocha et al. 2010).

To achieve a stable model run, an adaptive time step was used. Maximum time steps are 0.25 s and 0.2 s in the 2015 and 2016 model, respectively. The smaller time step for the 2016 episode was necessary due to higher wind speeds during the simulated period. A minimum time step of 0.0625 s was allowed for both model runs and used only on the first few time steps during initialization. After that, all model time steps were at their prescribed maximum. Both model runs were initialized at 0000 UTC (0200 local time) on their respective dates. Data starting at 6 hours

9

after model initialization were deemed usable. Full 3d-fields were written every 5 minutes. The data to be compared to the measurements is taken from profiles at four grid points in a 2×2 pattern at the measurements' location. These profiles were written at the model time resolution (0.25 s or 0.2 s) and later averaged in horizontal space and time. Data for the shown spectra of turbulence were treated accordingly.

The resulting modeling system drives a single LES domain directly with boundary conditions derived from the reanalysis data. The absence of any nesting processes lowers the cost in computing time so considerably that it is not outweighed by the use of the parameterizations listed above. One simulation with the described setup over two diurnal cycles took $\approx 10^5$ CPU hours. Muñoz-Esparza et al. (2017) require an order of magnitude more for their complex setup with four nested domains and similar parameterizations. We therefore recommend this modeling approach for cases where CPU power is sparse. It might also be used for small ensembles which is usually not done in LES.

b. Description of the virtual tower measurements

Three Doppler wind-Lidars (model StreamLine XP, Halo Photonics Ltd, Worcester, England) were arranged in a triangle with about 500 m spacing in between. The wind-Lidar is able to retrieve the speed of the air along a Lidar beam by measuring the Doppler shift in light backscattered by aerosols. All three Lidars simultaneously perform a scan at several heights along a vertical profile, producing a virtual measurement tower at that location. While a single Lidar can only measure speeds towards or away from its location, the combination of three is able to measure all three wind components (u, v, w), where u is the zonal, v the meridional and w the vertical wind component. The vertical resolution is 3 m up to a height of about 20 m above ground and 18 m up to a 1000 m above ground. The range above 1000 m was excluded because of detection

limitations, thought to be related to a decrease in particle density away from the surface that leads to decrease in backscattered laser light signal. The measured values of w in the lowest levels were considered unreliable and are therefore excluded from the evaluation. The highest temporal resolution for reliable values is one minute, aggregations for $10, 20, 30$ minutes were calculated from the one minute values. Data overlapping with the simulated period is from 0600 UTC 15 July to 0000 UTC 17 July (42 hours) for the 2015 measurement campaign and therefore contains a one and a half days, two sunsets and one whole night. The overlapping data for the 2016 campaign spans 32 hours, from 1600 UTC 6 July to 0000 UTC 8 July. In this dataset, there are two sunsets, one sunrise and one whole night and day. To perform a meaningful comparison, the measured wind speeds were linearly interpolated to the heights of the model levels.

3. Results and discussion

a. Instantaneous velocity fields

Here we evaluate the model results for two distinct cases: Figure 2 shows the instantaneous values for horizontal and vertical wind speed during a time period with low horizontal wind speeds, 1000 UTC 16 July 2015. The top panel of Figure 2 (a and d) show the values taken from the 30th model level ($\approx$ 300 m above ground). The plot for the vertical wind speed (Figure 2d) shows the typical situation for a boundary layer that is driven by buoyancy: spatially small areas with rising air are surrounded by larger patches of downdrafts. These cells of alternating up and downdrafts develop when the ratio between boundary layer height and Obukhov length, z_i/L, is strongly negative. The boundary layer height, z_i, is derived by searching for the largest gradient in the potential temperature (Sullivan et al. 1998). The Obukhov length, L, is a scaling parameter for the

11

surface layer:

$$L = \frac{-\overline{\Theta_v}u_*^3}{kg(\overline{w'\Theta_v'})_s}$$

Θ_v is the virtual potential temperature, u_* the friction velocity, k the von Karman constant (set to a value of 0.4 in WRF), g the gravitational constant and $\overline{w'\Theta_v'}_{vs}$ the kinematic heat flux at the surface. Deardorff (1972) finds cells at $z_i/L < -4.5$ and LeMone (1973) at $z_i/L < -10$. In the shown case, the bulk of the grid points exhibit values between -10 and -25. The total range of is from -60 to 0. Due to the inhomogeneities in terrain and land cover and the changing meteorological drivers, values of z_i/L can vary strongly between adjacent grid points. This is in contrast to idealized simulations, where all grid points are expected to behave equally.

The patterns in Figure 2 diverge from their ideal cell-like counterparts taken from idealized LES-Models (see e.g. Moeng et al. 2007) because of a horizontal wind speed larger than zero and inhomogeneities in surface properties and elevation. Modifications due to the underlying height gradients can be seen in the southwestern part of the domain where the mountain is located. On the southeastern slope is an accumulation of grid points with rising air (Figure 2d), possibly resulting from solar radiation coming in at an angle and heating the slope more than the surroundings. The thermals show rising speeds of up to 5 m s^{-1} while the sinking air never exceeds 3 m s^{-1}.

The lower two rows of Figure 2 show vertical cross-sections through the position of the virtual tower from west to east (b and e) and from south to north (c and f). Both cuts reveal an area of distinct shear at about 2000 m a.s.l. This originates from the reanalysis data used to drive the model, as the simulation can not produce shear on its own within this domain. It does not coincide with the boundary layer height, which is at $\approx$ 500 m to 700 m above ground during this time (evaluated by the gradient method applied to a spatial mean of 60 by 60 grid points at every grid point). The upper limit of the boundary layer is at the upper maximum extent of the thermal structures, especially visible in Figures 2e and f.

Figure 3 shows a time of high horizontal wind speeds (1600 UTC 7 July 2016) from a northerly direction. Due to the fact that WRF does not use any information about turbulence (e.g. vertical wind speeds or TKE) in the meteorological boundary conditions derived for real cases, turbulence has to develop within the domain. If horizontal wind speeds are larger than 0, this limitation of WRF manifests in areas of underdeveloped turbulence at the inflow edge that can be seen at the inflow edge of the domain, in the case of Figures 3a and d at the northern edge. When using WRF in an idealized mode and applying periodic boundary conditions, this problem does not arise, but when nesting another domain within the periodic domain, it can be noted. Several studies have described this behavior: Mirocha et al. (2013) used one way nesting in a neutral boundary layer, finding large streaks of underdeveloped turbulence at the inflow boundary with their extent depending on the used subgrid scale model, the geostrophic wind speed and the horizontal resolution of the model. They find that the NBA subgrid scale model used here shows the best results of the ones that are implemented in WRF and that a higher resolution allows for a quicker development of turbulence. The size of the undeveloped turbulence is dependent on the wind speed: The higher it is, the larger the area. Muñoz-Esparza et al. (2014b) find similar characteristics and propose the application of perturbing the temperature fields at the domain edges. This is applied to a realistic case in Muñoz-Esparza et al. (2014a) and to idealized neutral, stable and convective boundary layers in Muñoz-Esparza and Kosović (2018). It has to be noted that the authors listed here use geostrophic wind speeds of 5 and 10 m s^{-1} (Mirocha et al. 2013), 10 m s^{-1} (Muñoz-Esparza et al. 2014b) and 5, 10, and 15 m s^{-1} (Muñoz-Esparza and Kosović 2018) as boundary condition. These wind speeds are rather high and responsible for the size of the area of unresolved turbulence. In our case presented here, wind speeds rarely exceed 5 m s^{-1} in the boundary layer (cf. Figures 7 and 10, ignoring the nocturnal low-level jets that are above the boundary layer). This limits the size of the area of underdeveloped turbulence to what can be seen in Figure 3. Additionally,

13

Mirocha et al. (2014) note that the development of turbulence is favored by the presence of slopes in the domain and a positive heat flux at the surface, both of which exists in the modeling approach presented here.

The extent of the space in which no turbulence is developed can be seen on the right side of Figure 3c. In this case, with a mean wind speed of 3.4 m s^{-1}, it takes about 50 grid points distance from the inflow edge until turbulence develops near the ground and 150 grid points until turbulence is visible over the whole column. In cases with higher wind speeds the amount of grid points it takes until turbulence is developed fully is significantly larger. This has to be considered when setting the size of the model domain.

More information about the validity of the simulations and a sign that turbulence is indeed developed in the domain can be gathered from the spectrum of the frequencies of turbulence in Figure 4. Here we show the spectra from five different locations in the domain: all are on the same longitude in the center, but on different latitudes. *Far north* is 50 grid points away from the northern edge, *north* 150 grid points, *center* is in the center of the domain, and *south* and *far south* are in 350 and 450 grid points distance from the northern edge, respectively. The data is taken over two hours (1500-1700 UTC 7 July 2016), containing the time step shown in Figure 3. Before performing the Fourier transformation, the data is de-trended and tapered by the use of a cosine bell taper to the first and last 10 % of the data, following the instructions in Stull (1988) by using the function 'spec.taper' in the statistics software R. Shown are resolved frequencies in the horizontal wind speed. Only the point closest to the inflow edge shows a underdeveloped spectrum, where only the largest structures are resolved and spectral densities drop at high frequencies. All other points show similarly developed spectra with a distinctive inertial subrange. We therefore argue that the simulation results presented here are valid and can be used further, under the condition that grid points without developed turbulence are omitted from the analysis.

14

In terms of stability criteria, the period shown in Figure 3 is different to the one in Figure 2: Values for z_i/L are in the range of 0 to -13 over the whole domain. In contrast to cells forming, these values are within the range shown by LeMone (1973) and Deardorff (1972) to possibly produce roll like structures in the boundary layer. A comprehensive review on these rolls can be found in Etling and Brown (1993). There are elongated structures present in Figure 3, especially visible in the vertical wind speeds in the eastern part of the domain.

The simulated periods of twice 48 hours encompass several states the atmospheric boundary layer can be in. Instances of strongly and moderately convective periods are shown in Figures 2 and 3, respectively. Neutral stratification is a theoretical construct that happens very rarely in nature. It can be found at times when the unstable boundary layer turns stable or vice versa. These conditions are present during sunset and sunrise. The stable boundary layer on the other hand occurs in most nights. Stable nocturnal boundary layers are characterized by low wind speeds and a strong negative temperature gradient with height. The stable layering dampens turbulence, the turbulent structures are smaller than during day (e.g. Stull 1988). The smaller the turbulent structures, the smaller the model resolution has to be in order to resolve these structures.

Figure 5 shows spectra from times of strongly and moderately convective periods and a night period at the location of the virtual tower. To keep the data comparable, it is in all three cases taken from the 15 vertical levels below the averaged boundary layer height during the time considered. During day, the boundary layer height is determined by using the gradient method. The determination of the nocturnal boundary layer height cannot be accomplished by searching for the largest gradient in the potential temperature, because these gradients are within the boundary layer. Its height is limited by the residual layer above, in which the temperature gradients with height are small. As there is, to our knowledge, no formal method of determining the height of the nocturnal

15

boundary layer, we define it here as the height in which the gradient in potential temperature falls below 5% of the largest gradient measured beneath.

It is evident that turbulence in the moderately convective case shown in Figure 5 is best resolved. This is the time shown in Figure 3, characterized by high horizontal wind speeds. The spectrum for the strongly convective case is less well developed, there is less power on smaller scales. One reason is that turbulent structures that are predominantly caused by buoyancy are comparatively large. Another factor might be that this data is taken from the 2015 simulation that uses a slightly larger time step. Nevertheless, the inertial subrange is developed. During night the spectrum shows some scales of resolved turbulence. The total intensity is lower than in the two other cases, which is to be expected due to the smaller eddies present in the nocturnal boundary layer. An inertial subrange is discernible, but it is smaller than in the other two cases. In all three cases, the intensities in the vertical wind speed are higher than in the horizontal wind. According to Kaimal and Finnigan (1994), a spectrum shows atmospheric turbulence, when an inertial subrange is present and when the ratio in the intensities between streamwise and vertical wind speed in this inertial subrange is 4/3. In our shown case the ratio is always positive, but ranging between 1 and 4. This is because the frequency range of the inertial subrange has to be determined by hand and a small shift gives very different results. We also assume that the fact that the vertical resolution in this simulation is three times as fine as the horizontal resolution leads to more intensity in the vertical portion of the turbulence. We conclude from Figure 5 that the resolution of our models is sufficient for well-developed turbulence during daytime, but may be too coarse to properly resolve nighttime turbulence.

b. Comparison with virtual tower measurements

Figures 6 and 7 show the wind directions and wind speeds in the column above the virtual tower for a) the model and b) the measurement in 2015. The directions were calculated from the meridional and zonal wind components, averaged over 10 minutes. Both Figures only contain the time steps at which data is available for both the model and the virtual tower. Dotted vertical lines mark the timing of the sunset, dashed lines mark the sunrise.

The comparable period in 2015 contains 42 hours spanning from 0600 UTC 15 July to 0000 UTC 17 July. The first day, according to the measurements, is characterized by a well mixed daytime boundary layer with winds coming from northeast. These conditions are reached in the model by about 1500 UTC. Before that, the model shows an area of shear rising from the ground at 1000 UTC up to 1250 m a.s.l. at 1500 UTC. Above, the wind comes from northwest. After 1500 UTC the model represents the directions measured by the virtual tower. This coincides with growing wind speeds from 2 m s^{-1} to 5 m s^{-1} (see Figure 7). After sunset (dotted line), both the model and the measurement show a shift in the wind direction from northeast to east, and in the second half of the night, to south. During night time a shallow nocturnal boundary layer develops. It is characterized by mostly westerly wind direction and very low wind speeds. The nocturnal boundary layer grows to a depth of about 110 m in the model and 150 m in the measurement during the second half of the night. The height of the nocturnal boundary layer is again determined by using the method described in Chapter 3.

After sunrise (dashed line) the differences between model and measurement are largest: The observations show that the nocturnal boundary layer starts to transition into the daytime boundary layer after 0600 UTC near the ground with residuals remaining at around 200 m above ground. After the disappearance of the residuals the boundary layer becomes well mixed again with ho-

17

mogeneous directions (east) over the whole column. The model does not capture the growth of the nocturnal boundary layer up to the measured depth during night and simulates wind from south during the morning with a region of shear at 1000 m a.s.l. Starting at around 1100 UTC, the agreement between model and measurement improves. Both show a well mixed boundary layer with wind coming from northwest with increasing wind speeds during that time. During the evening, both show a shift from north over east to south. In the model this happens gradually while the changes in directions are very distinct in the measurements. In both cases, a new shallow nocturnal boundary layer develops.

As can be seen in Figure 7 the most prominent feature of the measurements of wind speeds is the low-level jet (LLJ, e.g. Stull 1988) during the first night at around 900 m a.s.l. It coincides with the top of the stable nocturnal boundary layer and is characterized by high wind speeds in relatively low heights. In many cases it is faster than the geostrophic wind above. The speed shown here grows immediately after sunset to 5 m s^{-1}. It reaches its maximum at 2300 UTC with just below 8 m s^{-1} with a vertical extent shrinking from almost 400 m to 100 m. The jet comes exclusively from the east and disappears suddenly at 2300 UTC, while the wind direction is shifting to the south. WRF-LES does capture the phenomenon of the LLJ, but the representation is insufficient. The simulated jet appears before sunset with the maximum approximately 5 hours early and 200 m higher. The vertical extent is strongly exaggerated and the maximum wind speeds are underestimated by about 2 m s^{-1}. Due to the shift in time, the simulated jet appears to come from northeast. A less pronounced LLJ can be found during the second night. The representation in the model shows the same shortcomings in timing, height and vertical extent as during the first occurrence.

The reason for the misrepresentation of the LLJ in the model data is the representation of the LLJ in the reanalysis data used as boundary conditions. The LLJ is not a local phenomenon and is

18

not created within the domain. In the reanalysis data used as boundary conditions the temporal and vertical resolutions are not high enough. The ERA-Interim reanalysis uses 38 vertical levels up to a height of 50 km. While no sign of the LLJ is visible in the boundary conditions for 1200 UTC 15 July 2015, it is clearly visible as higher wind speeds in the boundary conditions for the next time step at 1800 UTC. They reach 5.7 m s^{-1} in the fourth level at 820 m a.s.l. and 5.5 m s^{-1} and 4 m s^{-1} in the levels 6 and 7 (1060 and 1300 m a.s.l.). The 5th level in between at 930 m a.s.l. and those above the 7th and below the 4th show lower speeds of 3 m s^{-1}. 1800 UTC is exactly the time when the LLJ appears in the simulated data, as can be seen in Figure 7a. It also explains the vertical stretching, caused by the high wind speeds in the reanalysis from 820 to 1300 m a.s.l. and the lower maximum wind speeds of the simulated LLJ compared to the observed, caused by maximum wind speeds of 6.1 m s^{-1} in the reanalysis. In the next set of boundary conditions that is applied at 0000 UTC 16 July 2015, no signs of the LLJ are present in the data and the wind speeds in all essential vertical levels are below 3 m s^{-1}. For a proper representation of the LLJ in WRF-LES, boundary conditions with a high temporal, for example hourly, and a high vertical (<100 m) resolution are required.

The temporal course of the vertical wind speeds (not shown) behaves as is expected: during day and actively incoming solar radiation the 10-minute averaged vertical wind speeds easily reach ±2 m s^{-1} with alternating up- and downdrafts at the virtual tower location. After sunset the vertical motions are quickly dampened and stay below ±0.5 m s^{-1}. Directly after sunrise the turbulence starts weak and takes another 3 hours to reach the strength and vertical extent of the day before.

Density plots of the three discussed variables (direction, horizontal and vertical wind speed) in Figure 8 give a broader picture. They show only time steps and heights where both model data and measurement data is available. The direction is simulated well, model and measurement

19

show a distinct maximum around north. The secondary maximum at $100°$ in the measurements is shifted towards south in the model. Westerly directions are rare in measurement and model. The distributions of the horizontal wind speeds (Figure 8b) show two distinct features: the bulk of the wind speeds is slightly overestimated by the model (limit for the first quantile in the model: 1.69 m s^{-1}, measured: 1.33 m s^{-1}), while the maximum wind speeds are underestimated. These maximum wind speeds in the measurements (7.83 m s^{-1}) occur in the center of the LLJ that is, as described above, insufficiently represented in the model. The maximum wind speed in the model reaches 6.23 m s^{-1}. The simulated vertical wind speeds (Figure 8c) show a clear mean close to zero (–0.05 m s^{-1}), matching the theory of turbulence according to which vertical motions will average to zero over a sufficiently long time period. The mean of the measured values deviates from 0 and has a value of –0.15 m s^{-1}, hinting at possible surface inhomogeneities that favor downdrafts at the location. The model can not represent this. Both distributions of vertical wind speeds are skewed towards negative values. This is to be expected, since within one convective structure the area on which air rises is small compared to the area on which it sinks. If these structures pass by the virtual tower with the horizontal wind speed, the device will measure downdrafts for a longer time than updrafts.

The comparable period for the 2016 model covers 32 hours from 1600 UTC 6 July to 0000 UTC 8 July and therefore contains two sunsets and one sunrise. Both measurement and simulation show high wind speeds of up to 6 m s^{-1} (see Figure 10) coming from the north (Figure 9) before the first sunset. These high wind speeds were the reason for the required smaller model time step of the 2016 model in comparison to the 2015 model. The high wind speeds disappear during the first nighttime hours in the measurements, while a shallow nocturnal boundary layer develops. Simulated wind speeds diminish about one hour earlier. During the second half of the night, directions shift from north over east to south while the wind speeds are low. The model captures

this shift very well in timing and vertical extent. It also hints at an area of shear between 1000 m and 1200 m a.s.l. that can not be validated by the measurements. Both model and measurement show a growth of the nocturnal boundary layer depth during nighttime, while its maximum depth is again underestimated by the model. After sunrise the largest differences in the wind directions can be found. While the measurements show the dissipation of the nocturnal boundary layer due to beginning convection and northwesterly directions within the residuals, the model shows an extension of the conditions above the nocturnal boundary layer down to the ground with southerly directions. The position of the area of shear sinks down accordingly. It has to be noted that the determination of a wind direction from the horizontal wind components during times of low wind speeds, as they can be found here, are less reliable. Starting at 0900 UTC 7 July 2016, the agreement between model and measurement improves again. Both show northeasterly wind directions and growing wind speeds. The measured layer of the atmosphere is well mixed up to the maximum measurement height. After the second sunset the directions in model and measurement agree well, both showing the here often found pattern of a shift from north over east to south. The wind speeds, however, show the model limitation already mentioned in the 2015 data: the LLJ occurring between 800 m and 1000 m a.s.l. after sunset is misrepresented by the model. Here it again occurs earlier and before sunset and the vertical extent is exaggerated. Due to the shift in time, the direction of the LLJ (east) is also not represented in the simulation.

Conditions for the vertical wind speed are very similar to the 2015 model period. During the day, updrafts and downdrafts reach up to ±2 m s^{-1}. After sunset the vertical motions disappear, first near the ground while the air above the forming nocturnal boundary layer is still in motion, later over the whole column. After sunrise it takes about three hours until the high vertical speeds are reached again.

21

The density plots (Figure 11) for the three measured and simulated variables show a similar picture as in the 2015 model period: directions (Figure 11a) are mostly north. The secondary maximum of the simulated values at south represents the mismatch between model and measurement just after sunrise on 7 July 2016 (Figure 9). The two conclusions made from the wind speed data of the 2015 simulation hold true for 2016: the bulk amount of wind speeds is overestimated by the model (limit for the first quantile in the model: 1.51 m s^{-1}, measured: 1.23 m s^{-1}) and maximum wind speeds are underestimated: the model values only reach 5.2 m s^{-1} while speeds up to 6.59 m s^{-1} were measured during the simulation period. Figure 11c, showing the distributions of the vertical wind speeds, also confirms the findings from the 2015 model: the mean of the measured values is strongly negative (–0.25 m s^{-1}) in comparison to the simulation mean of –0.04 m s^{-1}. Both distributions are skewed towards negative values.

c. Additional value of model output compared to measurements

Considering the small size of the domain it is possible that WRF-LES with the setup described above primarily mixes the values prescribed by the boundary conditions with little connection to the actual properties of the selected area. To disprove this, a phenomenon within the model data has to be found that is spatially or temporally so confined that it can not originate from the boundary conditions. One such phenomenon can be seen on 0210 UTC 7 July 2016, where the measured wind speeds close to the ground are increasing from <2 m s^{-1} to 5 m s^{-1} for 50 minutes (Figure 10b). The phenomenon reaches 150 m in height. The wind is coming from the west. It is represented in the model data during the same time. The duration is overestimated (90 minutes from 0230 UTC to 0400 UTC), while height (70 m) and value of the wind speed (4 m s^{-1}) are underestimated. The direction is in agreement with the measurement. This phenomenon is not represented in the boundary conditions and has therefore to originate from the local conditions. Measurements

22

during other times have proven that this phenomenon occurs regularly, always shortly before sunrise and especially during summer. With just the point or column measurements the origin can not be reconstructed. Here, the four dimensional output of the model is a useful tool.

Figure 12 shows simulated wind speed data during the time of the phenomenon described above. The virtual tower, marked by the white spot, is positioned directly east of a small valley that cuts into the plateau in the western part of the model domain (see Figure 1b). Starting at 0130 UTC the conditions seen in Figure 12a begin to develop: significant katabatic flows from the mountain in the southwestern corner of the domain bring excess air towards the small valley. This forms a pool of cold air with a vertical extent of over 50 m on the ridge west of the virtual tower. This is further illustrated by Figure 13a, showing the deviations of potential temperature. The air here is up to 4 K colder than the average (9 °C) over the observed area up to 850 m a.s.l. and the horizontal wind speed is below 1 m s^{-1}. The cold air leaves the valley in zonal direction and accelerates on the plain. Data from the vertical wind speeds show constantly negative values of up to –0.6 m s^{-1} on the steepest part of the slope during the whole second half of the night. This in turn also increases the horizontal wind speeds near the ground. On the plain the flow is deflected towards the south (Figures 12a-c) in accordance with the wind direction just above the nocturnal boundary layer measured at the time (cf. Figure 9). Due to this deflection, the flow is not measured by the virtual tower until later. In the following hours (Figures 12d-f) the deflection is weakened and the flow takes a more straight western direction. It is during that time that the virtual tower measures increasing wind speeds in low heights. It is also the time in which the vertical extent of the flow reaches its maximum with about 70 m while it was more shallow before. Simultaneously, the depth of the cold air reservoir on top of the ridge shrinks to below 10 m and the deviations from the temperature mean are reduced from –3.2 °C to –2.7 °C (Figures 13d-f). The diminishing gradient is a hint that the cold pool is no longer replenished by flow from the mountain. Soon

after, the deflection takes an opposite sign and gives the flow a northward component (Figure 12g), making it pass by the virtual tower to the north. Vertical wind speeds during this time on the slope are still negative, but take an absolute lower value of –0.1 m s^{-1}. The virtual tower only measures this flow during a short moment in its transition from a southward to a northward deflection. Soon afterwards, the sunrise stops the katabatic flows from the hill (Figures 12h and i) and the flow in the plain vanishes. The temperature deviations on the hill drop to –1 °C in the last shown two time steps (Figure 13h and i), while these are also the time steps where the largest deviation from the mean occurs: in the very eastern part of the area shown in Figure 13, which is also the lowest part of the area, the temperatures are 4.3 °C cooler.

To analyze such micrometeorological events, the used simulation has to be run in a very high resolution: the horizontal resolution has to be fine enough to resolve the fine gradients in the elevation model and the vertical resolution has to have enough levels close to the ground that the shown strong temperature gradients can be resolved. LES are the only approach for this scale at the moment: the parameterizations that mesoscale models depend on can not be used in such high resolution and direct numerical simulations are computationally too expensive for an area the size of this.

4. Summary and conclusion

The study shows the setup and the application of WRF in LES mode for a real domain with realistic initial and boundary conditions, using high resolution land use and elevation maps and meteorological data from reanalysis. The LES domain was driven directly by the boundary conditions without further nesting, resulting in a setup that uses considerably less computing power than comparable nested setups.

24

LES and especially the employed subgrid scale model need a high vertical resolution for reliable results. This high resolution together with the terrain following coordinates used by WRF leads to challenges: steep slopes can easily cause violations of the Courant-Friedrichs-Lewy condition (Courant et al. 1967) and therefore disrupt the simulation. Shorter time steps and smoothing of the input elevation data can be a solution. In general, the setup of a high resolution WRF-LES domain for complex terrain has to be described as a process of trial and error. By changing the position and size of the domain, the distribution of the vertical levels or the time step, a working configuration can eventually be achieved.

The simulations represented the boundary condition mean values. The LES domain is forced by the meteorological drivers, limiting any significant deviation from the boundary conditions, even if they may have occurred between the ingestion intervals in the real-world. The strong dependence of the LES outcomes on the boundary conditions can be best seen at the transitions at dusk and dawn. For a proper representation of these atmospheric changes, boundary condition updates in higher temporal resolution are necessary. Within the LES domain the model develops typical LES flow structures. Due to the fact that this domain contains slopes, varying soil properties and changing radiation, the exact shape of these structures deviates from those produced within idealized LES. The problem of underdeveloped turbulence at the inflow edge of the domain is present, yet can be mitigated by removing affected grid points from the evaluation. As the size of this area depends on horizontal wind speed, this modeling approach is mostly suited for times of average wind speeds < 5 m s^{-1}. For higher wind speeds we recommend to expand the domain in the streamwise direction to increase the amount of grid points where turbulence can develop.

The two ScaleX campaigns from 2015 and 2016 provide a unique dataset for the evaluation of the model data. In the presented text we compared the model results to the measurements of an innovative measurement system, a virtual tower, consisting of three Doppler-Lidar devices, that is

25

able to measure the wind components in the boundary layer in high vertical and temporal resolution. Compared to these measurements the model shows that it is sufficiently able to represent the meteorological conditions of the area. Simulated patterns in wind speed and direction are in accordance with the measurements. Weaknesses are in the representation of the nocturnal boundary layer height that is underestimated in the model and the LLJs which are insufficiently represented in the boundary conditions.

The most promising approach for improving the modeling setup is the use of boundary conditions with a higher resolution, especially temporal. Ideally, these boundary conditions are downscaled online by nesting the LES-domain in mesoscale domains, yet this increases the required computing time substantially. The vertical nesting capabilities of the newer WRF versions might be a big step in this direction.

The fact that WRF-LES simulated the locally and temporarily confined phenomenon of increased wind speeds in low heights due to katabatic flows at night shows that the described modeling approach is able to produce local phenomena that are not present in the boundary conditions. For such cases the output of a model is a valuable addition to measurements. Due to its four dimensional structure it can provide information about spatial or temporal developments. This information can be used in urban management, by identifying and preserving flows of fresh air from the surroundings to improve the air quality. In the case of the presented area, which is characterized by dairy farming, the information can be used to build stables in a way that minimizes the odor nuisance for neighboring residential areas. Around airports, the data from realistic LES could be used to identify hot spots where strong turbulent motions develop, improving flight safety. With increasing computing power these applications are well within reach and the lower computational costs of the approach presented here even allows for studies on all kinds of weather conditions.

26

References

Aitken, M. L., B. Kosović, J. D. Mirocha, and J. K. Lundquist, 2014: Large eddy simulation of wind turbine wake dynamics in the stable boundary layer using the Weather Research and Forecasting model. *Journal of Renewable and Sustainable Energy*, **6 (3)**, 033 137.

Andren, A., A. R. Brown, P. J. Mason, J. Graf, U. Schumann, C.-H. Moeng, and F. T. Nieuwstadt, 1994: Large-eddy simulation of a neutrally stratified boundary layer: A comparison of four computer codes. *Quarterly Journal of the Royal Meteorological Society*, **120 (520)**, 1457–1484.

Basu, S., and A. Lacser, 2017: A cautionary note on the use of Monin–Obukhov similarity theory in very high-resolution large-eddy simulations. *Boundary-Layer Meteorology*, **163 (2)**, 351–355.

Basu, S., and F. Porté-Agel, 2006: Large-eddy simulation of stably stratified atmospheric boundary layer turbulence: a scale-dependent dynamic modeling approach. *Journal of the Atmospheric Sciences*, **63 (8)**, 2074–2091.

Beare, R. J., 2008: The role of shear in the morning transition boundary layer. *Boundary-Layer Meteorology*, **129 (3)**, 395–410.

27

Beare, R. J., and Coauthors, 2006: An intercomparison of large-eddy simulations of the stable boundary layer. *Boundary-Layer Meteorology*, **118 (2)**, 247–272.

Bou-Zeid, E., C. Meneveau, and M. B. Parlange, 2004: Large-eddy simulation of neutral atmospheric boundary layer flow over heterogeneous surfaces: Blending height and effective surface roughness. *Water Resources Research*, **40 (2)**, doi:10.1029/2003wr002475.

Bou-Zeid, E., J. Overney, B. D. Rogers, and M. B. Parlange, 2009: The effects of building representation and clustering in large-eddy simulations of flows in urban canopies. *Boundary-Layer Meteorology*, **132 (3)**, 415—-436, doi:10.1007/s10546-009-9410-6.

Catalano, F., and C.-H. Moeng, 2010: Large-eddy simulation of the daytime boundary layer in an idealized valley using the Weather Research and Forecasting numerical model. *Boundary-Layer Meteorology*, **137 (1)**, 49–75.

Chow, F. K., and R. L. Street, 2009: Evaluation of turbulence closure models for large-eddy simulation over complex terrain: Flow over Askervein Hill. *Journal of Applied Meteorology and Climatology*, **48 (5)**, 1050—-1065, doi:10.1175/2008jamc1862.1.

Chu, X., L. Xue, B. Geerts, R. Rasmussen, and D. Breed, 2014: A case study of radar observations and WRF LES simulations of the impact of ground-based glaciogenic seeding on orographic clouds and precipitation. Part I: Observations and model validations. *Journal of Applied Meteorology and Climatology*, **53 (10)**, 2264–2286.

CLC, 2000: Corine land cover 100 m, ver. 5. European Environment Agency (©EEA, Copenhagen).

Courant, R., K. Friedrichs, and H. Lewy, 1967: On the partial difference equations of mathematical physics. *IBM journal of Research and Development*, **11 (2)**, 215–234.

Crosman, E. T., and J. D. Horel, 2012: Idealized large-eddy simulations of sea and lake breezes: Sensitivity to lake diameter, heat flux and stability. *Boundary-Layer Meteorology*, **144 (3)**, 309—-328, doi:10.1007/s10546-012-9721-x.

Daniels, M. H., K. A. Lundquist, J. D. Mirocha, D. J. Wiersema, and F. K. Chow, 2016: A new vertical grid nesting capability in the Weather Research and Forecasting (WRF) model. *Monthly Weather Review*, **144 (10)**, 3725—-3747, doi:10.1175/MWR-D-16-0049.1.

Deardorff, J. W., 1970: A three-dimensional numerical investigation of the idealized planetary boundary layer. *Geophysical and Astrophysical Fluid Dynamics*, **1 (3-4)**, 377–410.

Deardorff, J. W., 1972: Numerical investigation of neutral and unstable planetary boundary layers. *Journal of the Atmospheric Sciences*, **29 (1)**, 91–115.

ECMWF, 2009, updated monthly: ERA-Interim Project. Research Data Archive at the National Center for Atmospheric Research, Computational and Information Systems Laboratory, Boulder CO, Research Data Archive at the National Center for Atmospheric Research, Computational and Information Systems Laboratory, doi:10.5065/D6CR5RD9.

Etling, D., and R. Brown, 1993: Roll vortices in the planetary boundary layer: A review. *Boundary-Layer Meteorology*, **65 (3)**, 215–248.

Hattori, Y., C.-H. Moeng, H. Hirakuchi, S. Ishihara, S. Sugimoto, and H. Suto, 2010: Numerical simulation of turbulence structures in the neutral atmospheric surface layer with a mesoscale moteorological model, WRF. *Proceedings of the fifth International Symposium on Computational Wind Engineering*, Vol. 5, 385.

Hong, S.-Y., J. Dudhia, and S.-H. Chen, 2004: A revised approach to ice microphysical processes for the bulk parameterization of clouds and precipitation. *Monthly Weather Review*, **132 (1)**, 103–120.

Huang, J., and E. Bou-Zeid, 2013: Turbulence and vertical fluxes in the stable atmospheric boundary layer. Part I: A large-eddy simulation study. *Journal of the Atmospheric Sciences*, **70 (6)**, 1513—-1527, doi:10.1175/jas-d-12-0167.1.

Iacono, M. J., J. S. Delamere, E. J. Mlawer, M. W. Shephard, S. A. Clough, and W. D. Collins, 2008: Radiative forcing by long-lived greenhouse gases: Calculations with the AER radiative transfer models. *Journal of Geophysical Research: Atmospheres*, **113 (D13)**.

Kaimal, J. C., and J. J. Finnigan, 1994: *Atmospheric boundary layer flows: their structure and measurement*. Oxford University Press.

Kosović, B., 1997: Subgrid-scale modelling for the large-eddy simulation of high-Reynolds-number boundary layers. *Journal of Fluid Mechanics*, **336**, 151–182.

Kosović, B., and J. A. Curry, 2000: A large eddy simulation study of a quasi-steady, stably stratified atmospheric boundary layer. *Journal of the Atmospheric Sciences*, **57 (8)**, 1052–1068.

Lang, M., A. Gohm, and J. Wagner, 2015: The impact of embedded valleys on daytime pollution transport over a mountain range. *Atmospheric Chemistry and Physics*, **15 (20)**, 11 981–11 998.

LeMone, M. A., 1973: The structure and dynamics of horizontal roll vortices in the planetary boundary layer. *Journal of the Atmospheric Sciences*, **30 (6)**, 1077–1091.

Lundquist, K. A., F. Chow, and J. Lundquist, 2010: Numerical errors in flow over of steep topography: analysis and alternatives. *14th Conference on Mountain Meteorology*.

Mirocha, J., G. Kirkil, E. Bou-Zeid, F. K. Chow, and B. Kosović, 2013: Transition and equilibration of neutral atmospheric boundary layer flow in one-way nested large-eddy simulations using the Weather Research and Forecasting Model. *Monthly Weather Review*, **141 (3)**, 918—-940, doi:10.1175/mwr-d-11-00263.1.

Mirocha, J., B. Kosović, and G. Kirkil, 2014: Resolved turbulence characteristics in large-eddy simulations nested within mesoscale simulations using the Weather Research and Forecasting model. *Monthly Weather Review*, **142 (2)**, 806–831.

Mirocha, J., J. Lundquist, and B. Kosović, 2010: Implementation of a nonlinear subfilter turbulence stress model for large-eddy simulation in the Advanced Research WRF model. *Monthly Weather Review*, **138 (11)**, 4212–4228.

Moeng, C., J. Dudhia, J. Klemp, and P. Sullivan, 2007: Examining two-way grid nesting for large eddy simulation of the PBL using the WRF model. *Monthly Weather Review*, **135 (6)**, 2295–2311.

Moeng, C.-H., 1984: A large-eddy-simulation model for the study of planetary boundary-layer turbulence. *Journal of the Atmospheric Sciences*, **41 (13)**, 2052–2062.

Moeng, C.-H., 1986: Large-eddy simulation of a stratus-topped boundary layer. Part I: Structure and budgets. *Journal of the Atmospheric Sciences*, **43 (23)**, 2886–2900.

Muñoz-Esparza, D., and B. Kosović, 2018: Generation of inflow turbulence in large-eddy simulations of non-neutral atmospheric boundary layers with the cell perturbation method. *Monthly Weather Review*, **146 (6)**, 1889–1909.

Muñoz-Esparza, D., B. Kosović, C. García-Sánchez, and J. van Beeck, 2014a: Nesting turbulence in an offshore convective boundary layer using large-eddy simulations. *Boundary-layer meteorology*, **151 (3)**, 453–478.

Muñoz-Esparza, D., B. Kosović, J. Mirocha, and J. van Beeck, 2014b: Bridging the transition from mesoscale to microscale turbulence in numerical weather prediction models. *Boundary-layer meteorology*, **153 (3)**, 409–440.

Muñoz-Esparza, D., J. K. Lundquist, J. A. Sauer, B. Kosović, and R. R. Linn, 2017: Coupled mesoscale-LES modeling of a diurnal cycle during the CWEX-13 field campaign: From weather to boundary-layer eddies. *Journal of Advances in Modeling Earth Systems*, **9 (3)**, 1572–1594.

NASA/METI/AIST/Japan Spacesystems, and U.S./Japan ASTER Science Team, 2009: ASTER global digital elevation model. distributed by NASA EOSDIS Land Processes DAAC, doi:10.5067/ASTER/ASTGTM.002.

Nieuwstadt, F. T., P. J. Mason, C.-H. Moeng, and U. Schumann, 1993: Large-eddy simulation of the convective boundary layer: A comparison of four computer codes. *Turbulent Shear Flows 8*, Springer, 343–367.

Nunalee, C. G., B. Kosović, and P. E. Bieringer, 2014: Eulerian dispersion modeling with WRF-LES of plume impingement in neutrally and stably stratified turbulent boundary layers. *Atmospheric environment*, **99**, 571–581.

Rai, K., L. K. Berg, B. Kosović, J. D. Mirocha, M. S. Pekour, and W. J. Shaw, 2017: Comparison of measured and numerically simulated turbulence statistics in a convective boundary layer over complex terrain. *Boundary-Layer Meteorology*, **163 (1)**, 69–89.

Saiki, E. M., C.-H. Moeng, and P. P. Sullivan, 2000: Large-eddy simulation of the stably stratified planetary boundary layer. *Boundary-Layer Meteorology*, **95 (1)**, 1–30.

Siebesma, A. P., and Coauthors, 2003: A large eddy simulation intercomparison study of shallow cumulus convection. *Journal of the Atmospheric Sciences*, **60 (10)**, 1201–1219.

Skamarock, W., and Coauthors, 2008: A description of the advanced research WRF version 3: NCAR/TN-475. *STR, NCAR technical note. NCAR, Boulder*, **88**.

Stull, R. B., 1988: *An introduction to boundary layer meteorology*, Vol. 13. Springer Science & Business Media.

Sullivan, P. P., C.-H. Moeng, B. Stevens, D. H. Lenschow, and S. D. Mayor, 1998: Structure of the entrainment zone capping the convective atmospheric boundary layer. *Journal of the atmospheric sciences*, **55 (19)**, 3042–3064.

Talbot, C., E. Bou-Zeid, and J. Smith, 2012: Nested mesoscale large-eddy simulations with WRF: Performance in real test cases. *Journal of Hydrometeorology*, **13 (5)**, 1421—-1441, doi:10.1175/jhm-d-11-048.1.

Wagner, J., A. Gohm, and M. Rotach, 2015: The impact of valley geometry on daytime thermally driven flows and vertical transport processes. *Quarterly Journal of the Royal Meteorological Society*, **141 (690)**, 1780–1794.

Wolf, B., and Coauthors, 2017: The SCALEX campaign: Scale-crossing land surface and boundary layer processes in the TERENO-preAlpine Observatory. *Bulletin of the American Meteorological Society*, **98 (6)**, 1217–1234.

Xue, L., X. Chu, R. Rasmussen, D. Breed, and B. Geerts, 2016: A case study of radar observations and WRF LES simulations of the impact of ground-based glaciogenic seeding on orographic

clouds and precipitation. Part II: AgI dispersion and seeding signals simulated by WRF. *Journal of Applied Meteorology and Climatology*, **55 (2)**, 445–464.
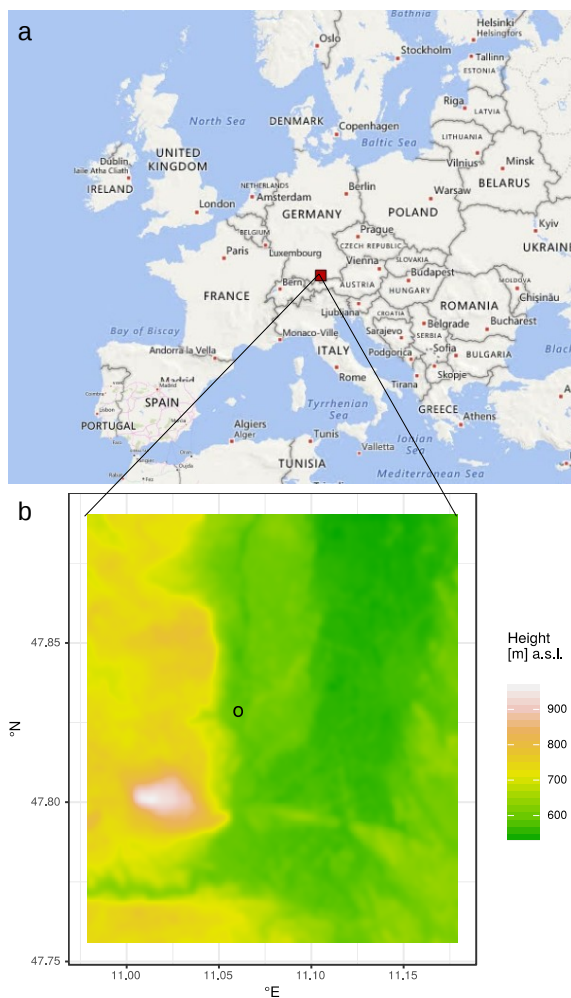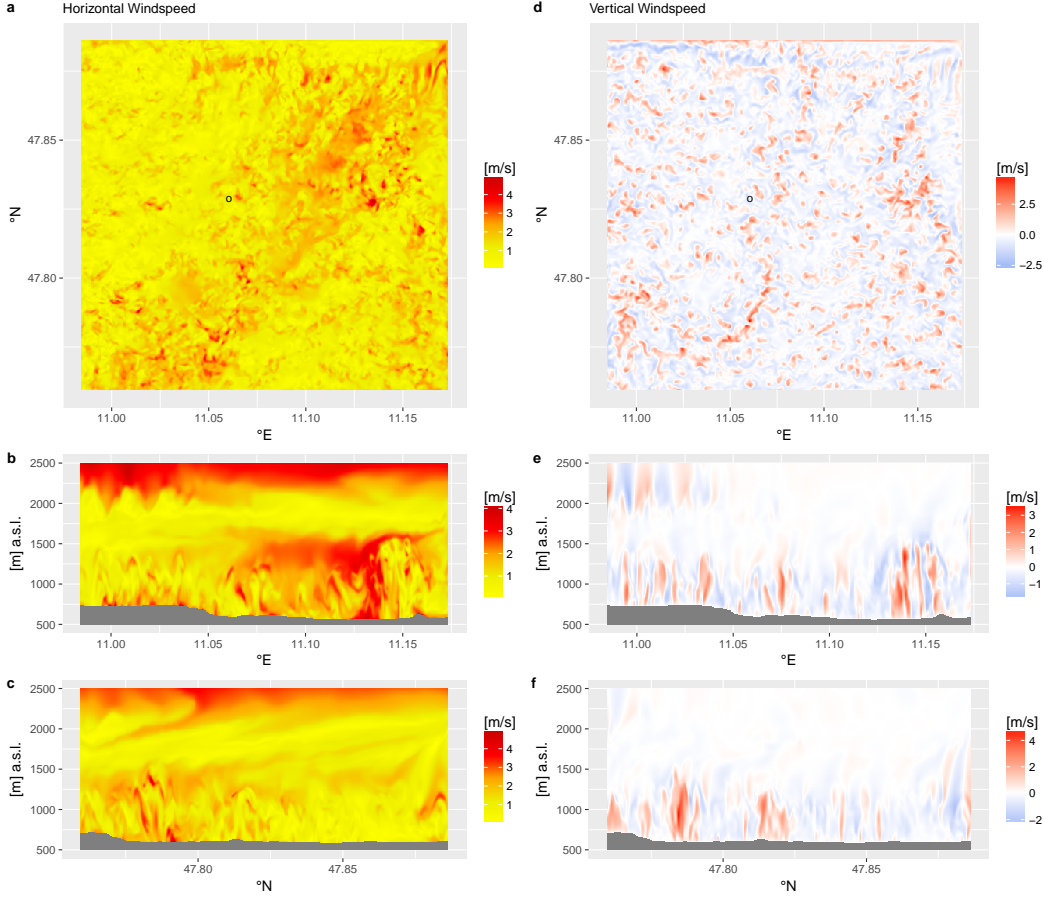
LIST OF FIGURES

35

FIG. 1. a: position of the model domain in Europe (Source: Bing Maps). b: orography of the modeled area. Heights are in meters above sea level (a.s.l.). The circle shows the position of the virtual tower.

FIG. 2. Instantaneous values of wind components (a-c: horizontal wind speed, d-f: vertical wind speed) for a time step of low horizontal wind speeds (1000 UTC 16 July 2015). a and d: values from the 30th vertical model level ($\approx$ 300 m above ground). The circle shows the position of the virtual tower. b and e: cut from west to east through the virtual tower position. c and f: cut from south to north through the virtual tower position.
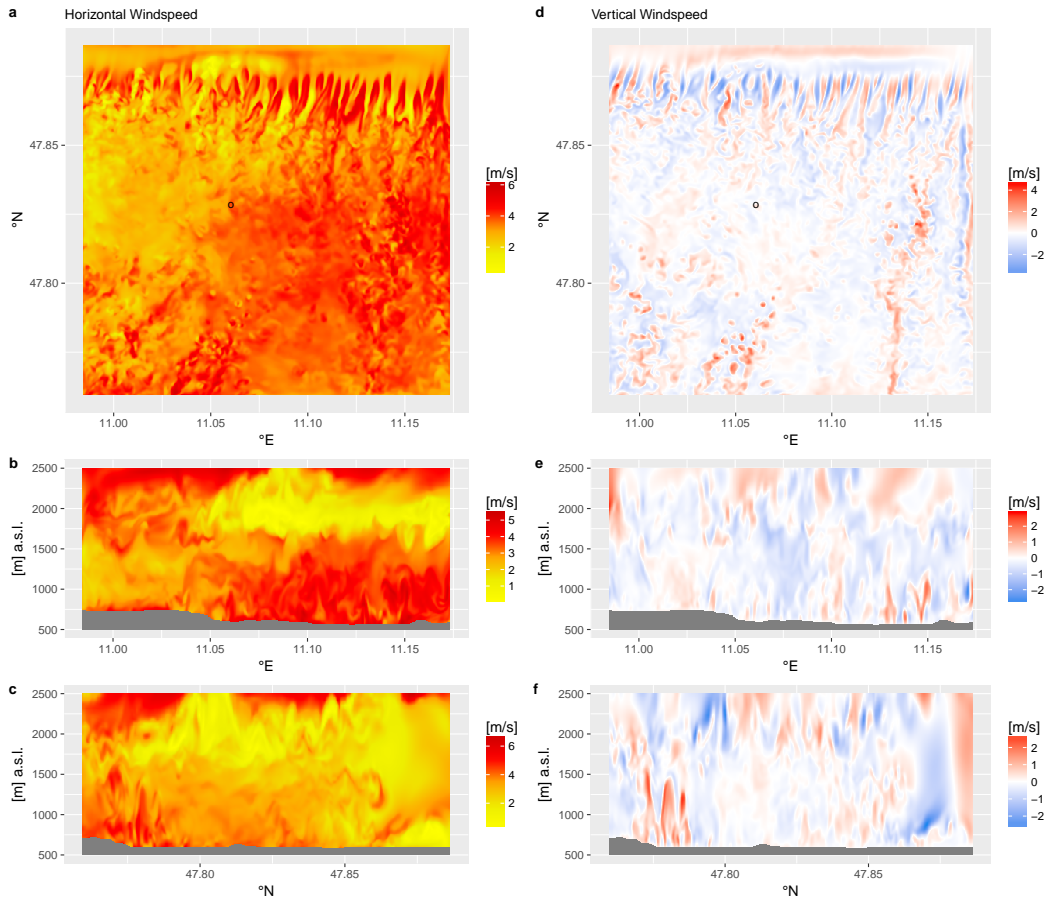
FIG. 3. Instantaneous values of wind components (a-c: horizontal wind speed, d-f: vertical wind speed) for a time step of high horizontal wind speeds (1600 UTC 7 July 2016). Same structure as in figure 2
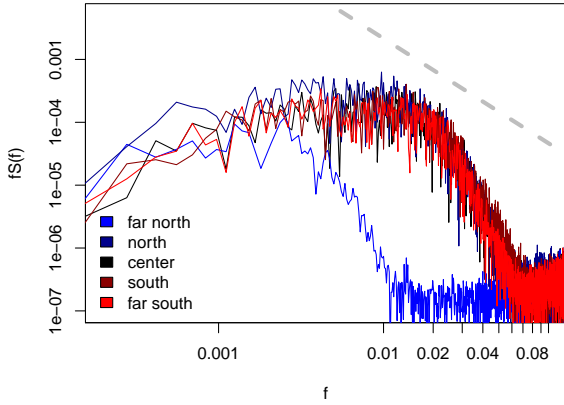
FIG. 4. Spectra of horizontal wind speed at 5 distances from the northern edge: 50 (far north), 150 (north), 250 (center), 350 (south) and 450 (far south) grid points. Data taken from 2 hours of model data (1500-1700 UTC 7 July 2016) and averaged over 3 vertical levels (55 m to 77 m over ground). The grey dashed line is $f^{-\frac{5}{3}}$. It marks the inertial subrange.
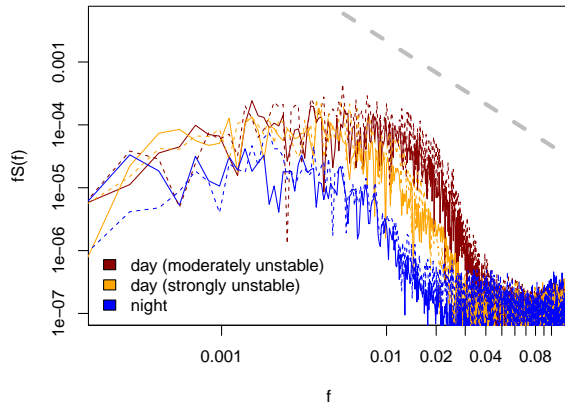
FIG. 5. Spectra of horizontal (solid line) and vertical (dashed line) wind speeds for periods of strongly convective, moderately convective and stable (night) periods. Values taken from 15 vertical levels down from the average boundary layer height over a period of 2 hours. The grey dashed line is $f^{-\frac{5}{3}}$.
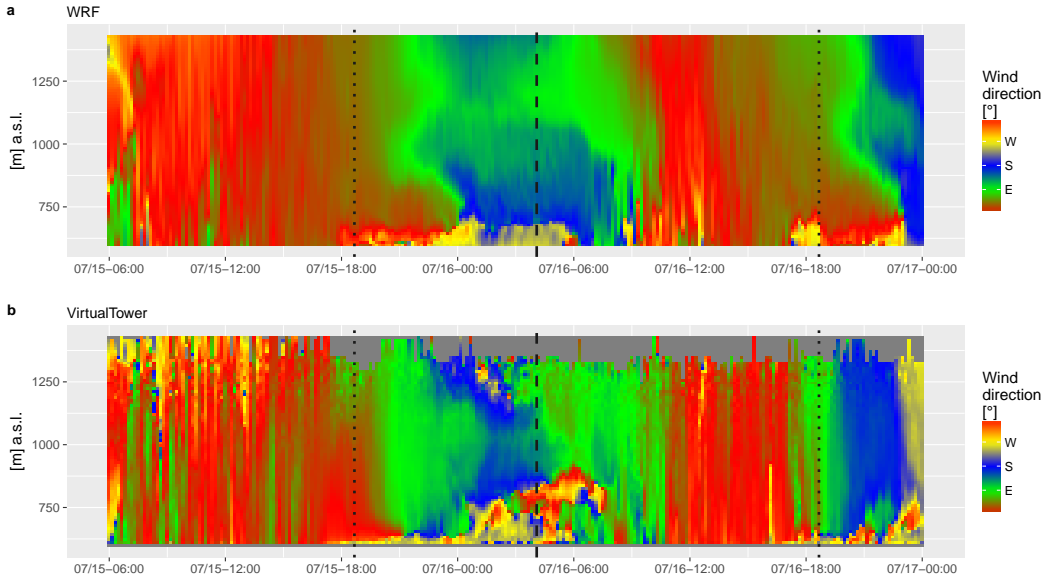
FIG. 6. Wind directions from a) WRF-LES and b) the virtual tower for the 2015 simulation period. Model data taken from 4 grid points in a 2x2 pattern and horizontally averaged. Values are temporally averaged to 10 minute means. Virtual tower data linearly interpolated to model levels. Dashed lines: sunrise, dotted lines: sunset. Time steps are on the x-axis, heights above sea level on the y-axis. Values of direction are color coded, NA values due to the limited measurement height of the virtual tower are dark grey.
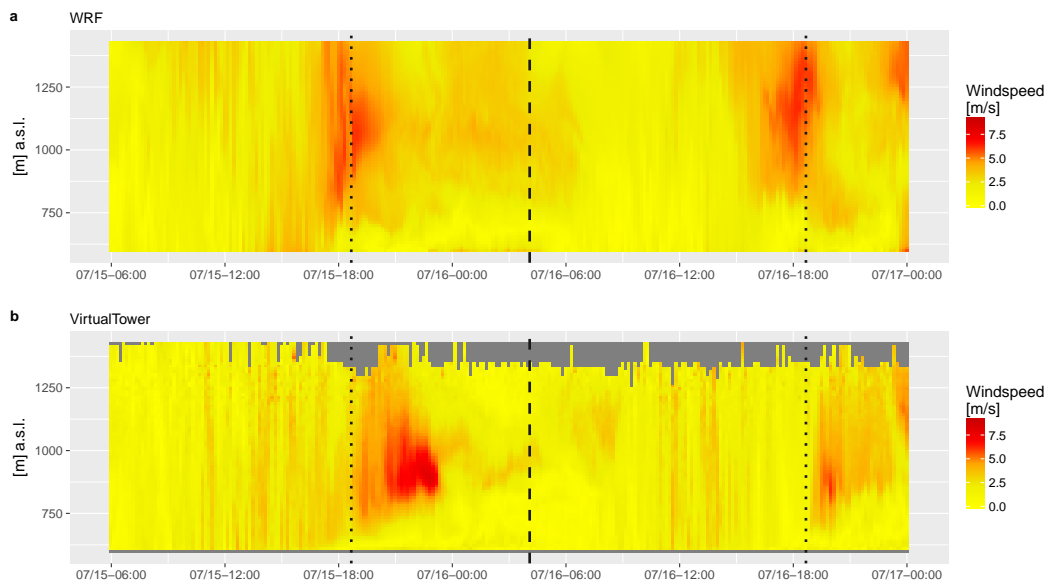
FIG. 7. Wind speeds from a) WRF-LES and b) the virtual tower for the 2015 simulation period.
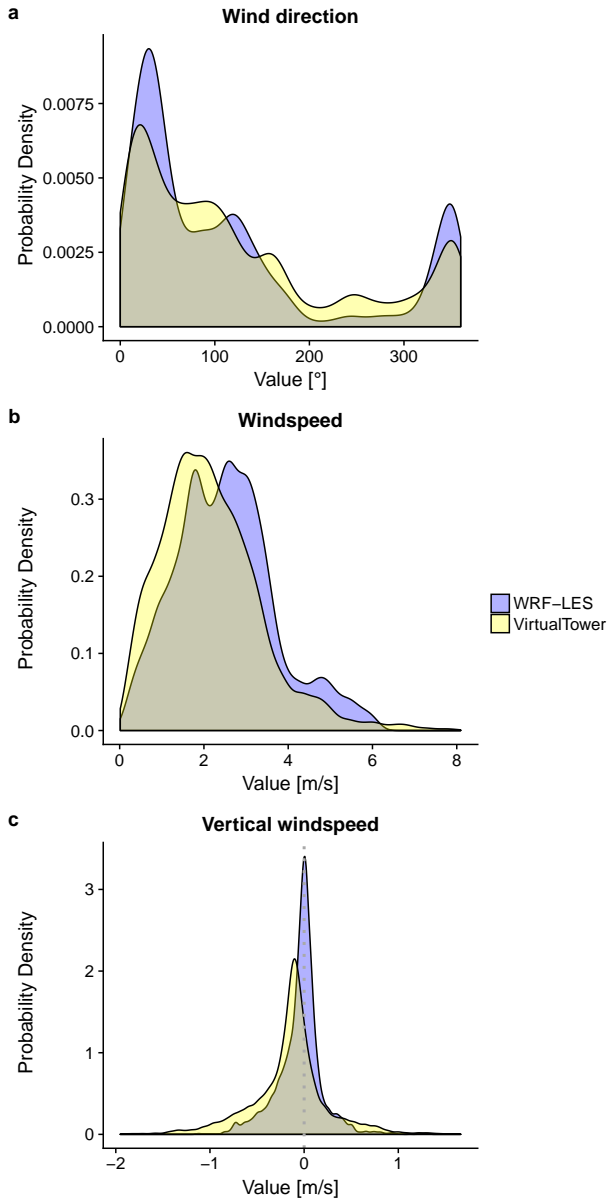
FIG. 8. Density plots of measured and simulated values for a) wind direction, b) horizontal wind speed and c) vertical wind speed from the 2015 simulation period.
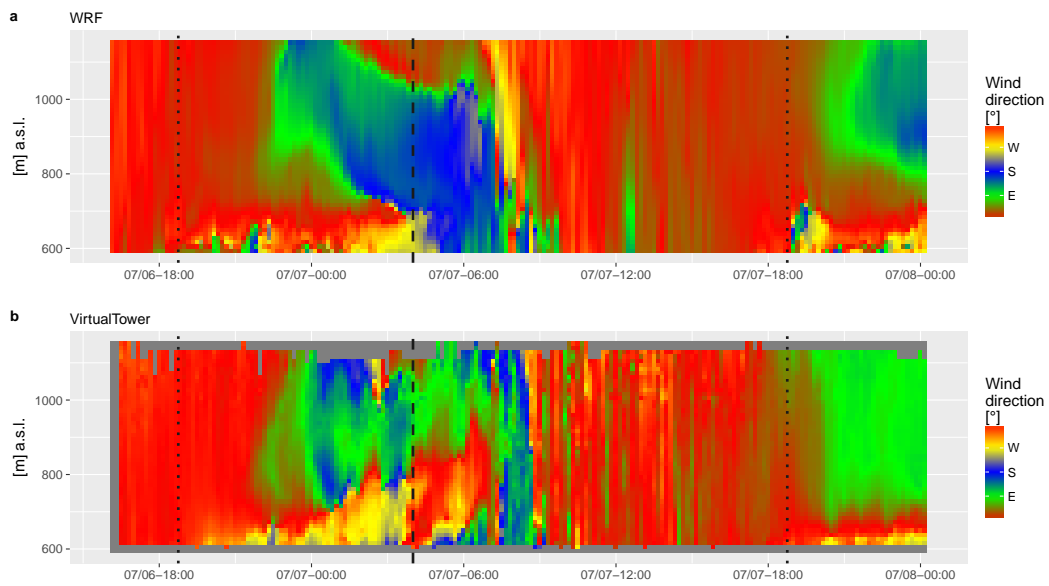
FIG. 9. Wind directions from a) WRF-LES and b) the virtual tower for the 2016 simulation period.
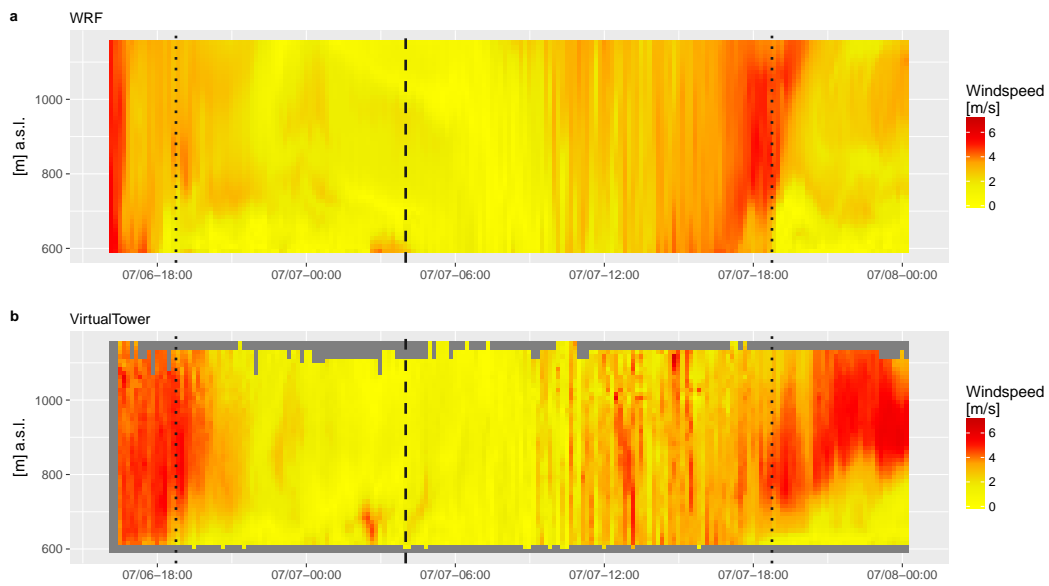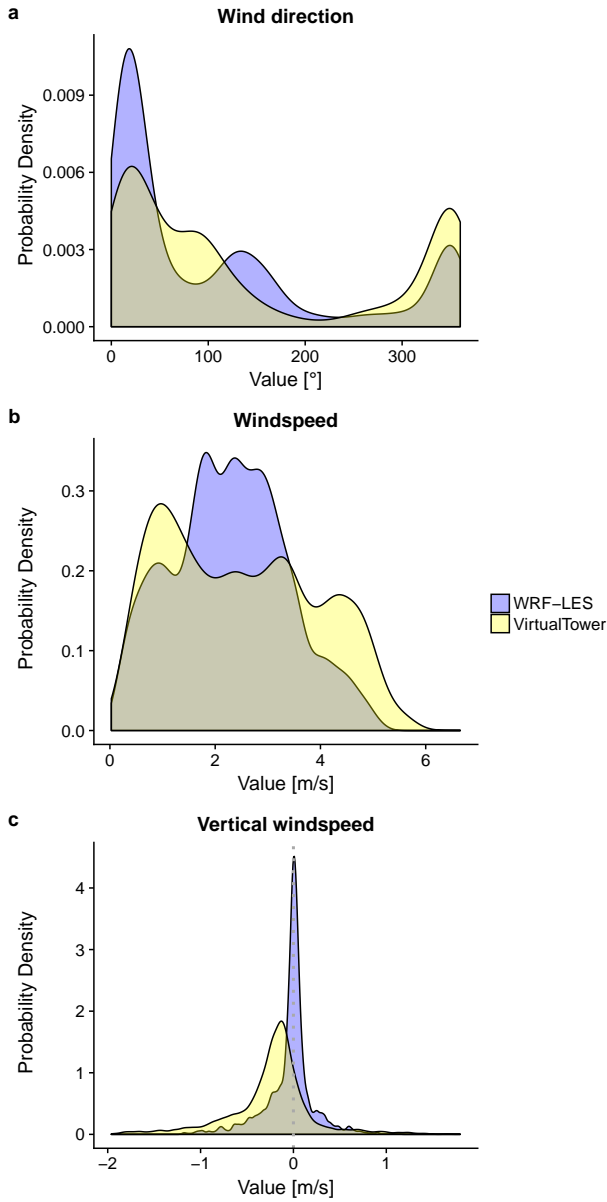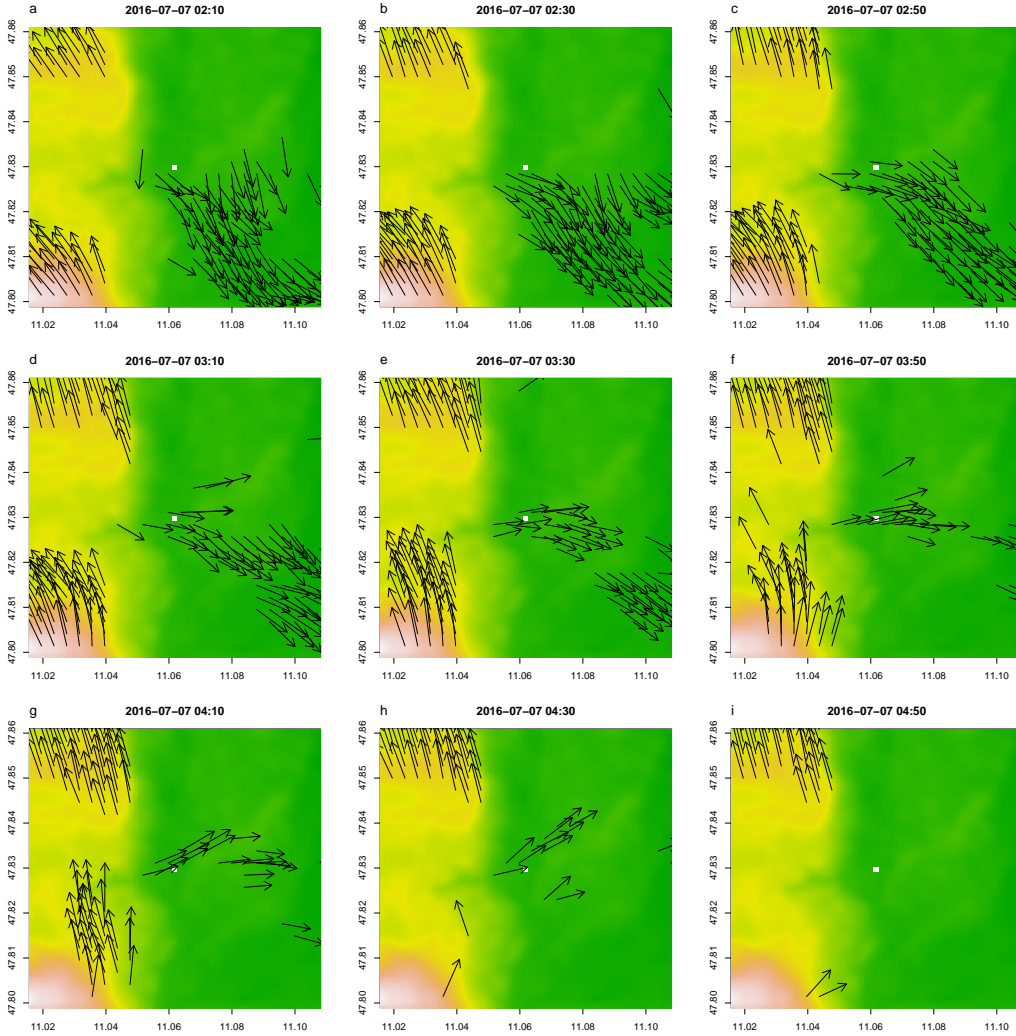
45

FIG. 10. Wind speeds from a) WRF-LES and b) the virtual tower for the 2016 simulation period.

FIG. 11. Density plots of measured and simulated values for a) wind direction, b) horizontal wind speed and c) vertical wind speed from the 2016 simulation period.

FIG. 12. Temporal development of the flow passing the virtual tower (marked by the white spot) in the early morning of 7 July 2016. Arrows are scaled by the wind speed. Speed data averaged over four vertical levels between 33 m and 66 m above ground. Arrows are only drawn for speeds >1.4 m s^{-1}
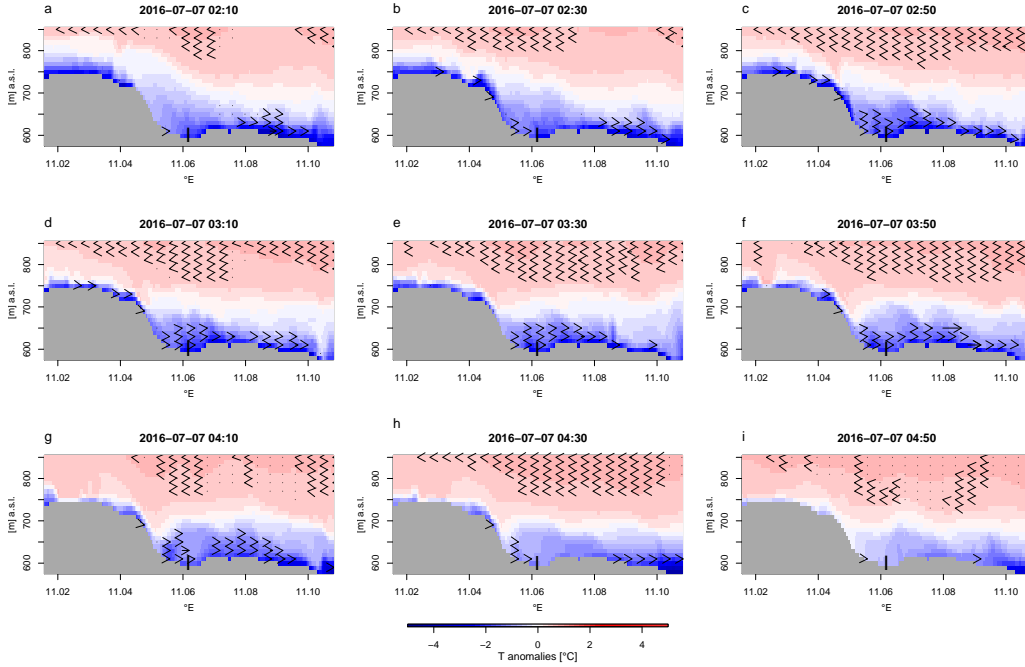
FIG. 13. Temporal development of the potential temperature deviations for the time steps shown in Figure 12. The deviations are calculated from the mean of all data points shown in the 9 Figures (temporal and spatial averaging). Cut from west to east through the position of the virtual tower (the black "I"). Arrows are drawn where horizontal wind speeds exceed 1.4 m s^{-1}